UNIVERSITÄT
BAYREUTH

Master Thesis

Mitigation of the Cancellation Problem in local gyrokinetic Simulations

Manuel Lippert

Submission Date: September 30, 2024

Physics Department at the University of Bayreuth

Supervisors:
Prof. Arthur G. Peeters
Dr. Florian Rath

★ 07.07.2020 - † 09.08.2024

This thesis is dedicated to my cat **Leo**
who is part of our family since July 2020.
He is the kindest cat I ever owned.
During the pandemic we got very close.
I will miss our walks together and your company in my life.

I love you.

Manuel Lippert

Acknowledgement

First, I would like to extend my greatest gratitude to my supervisors Prof. Arthur Peeters and Dr. Florian Rath. I would like to thank both of you for your guidance and support during the writing process of this thesis.

I would like to thank René Meißner for the access to the festus cluster and Markus Hilt for the great technical support.

Also, I would like to thank my best friend, Paul Schwanitz, for his support in many situations and the good discussions in- and outside of academia. In addition, I would like to thank Anna-Maria Pleyer and Fabian Eller for the great time of sharing the office together.

I thank my sister Cornelia Lippert for proofreading this thesis, which shows me that I still have to improve my English spelling.

Outside of academia, I would like to extend my gratitude to my parents, my brother, his wife and daughter, my sister and my girlfriend for their encouragement, endurance and support while writing this thesis.

Abstract

The so-called cancellation problem limits electromagnetic gyrokinetic simulations to low plasma beta values and long perpendicular turbulent length scales. To mitigate this problem a new numerical scheme was found for global nonlinear gyrokinetic simulations. This scheme relies on the introduction of an electromagnetic additional field, the plasma induction, through Faraday's law. The implementation of Faraday's law into GKW results in the calculation of the gyrocenter distribution, which before needed to be modified. For local linear simulations the computational time increases by 10 %.

With local linear benchmarks the validity of the implementation was proven plausible. However, the cancellation problem could not be solved by the plasma induction in linear simulations. Simulations using the nonlinear version of GKW showed the trend that the implementation is valid, but they could not be finished due to time constraints.

Zusammenfassung

Das sogenannte Auslöschungsproblem limitiert elektromagnetische gyrokinetische Simulationen auf kleine Plasma Beta Werte und lange senkrechte turbulente Längenskalen. Um das Auslöschungsproblem zu vermeiden, wurde ein neues nummerische Schema in globalen nichtliniearen Simulationen gefunden. Dieses Schema führt zusätzliches electromagnetisches Feld, genannt Plasma Induktion, über das Faradaysche Gesetz ein. Die Implementierung des Faradayschen Gesetzes hat zur Folge, dass GKW nun die Verteilungsfunktion im Gyrozentrum unmodifiziert berechnen kann. Für lokal lineare Simulationen erhöhte sich die Laufzeit des Codes um 10 %.

Die Validität der Implementierung wurde mit lokalen linearen Simulationen geprüft. Dennoch konnte das Auslöschungsproblem nicht behoben werden. Simulationen, welche die nichtlineare Version von GKW nutzen, zeigten einen Trend, dass die Implementierung valide ist, aber sie konnten nicht abgeschlossen werden aufgrund zeitlicher Einschränkungen.

Declaration

The author states that every information, regarding this thesis can be found under the GitHub Repository with the link `https://github.com/ManeLippert/Masterthesis-Parallel-Electric-Field`.

Contents

CHAPTER

1

Motivation

Plasma can be described in various theoretical models. The main two models are the Magnetohydrodynamics and the Kinetic Model. The key differences will be briefly explained in the following.

- **Magnetohydrodynamics (MHD):**
  In Magnetohydrodynamics the plasma will be described as an electric conductiv fluid which carries current. Here, the electrons and ions are two mixed fluids expressed in the two-fluid theory.
- **Kinetic Model:**
  In the Kinetic Model the plasma will be described in the six-dimensional phase space through the Vlasov equation. In combination with the Maxwell's equations it is possible to describe the dynamics of the plasma as the Vlasov-Maxwell system.

In both descriptions macroscopic quantities will be used, i.e. density, velocity of the fluid and temperature. For this thesis only the kinetic description will be used.

However, the plasma beta is considered to be one of the fundamental dimensionless parameters in plasma physics, due to its relevance for the outcome, the fusion rate ($\sim \beta^2$), the bootstrap fraction ($\sim \beta$), the MHD stability and the confinement quality of fusion devices such as a Tokamak. Also, the plasma beta is an indicator for the relevance of electromagnetic effects in a gyrokinetic system, since electromagentic fields vanish in the limit $\beta \to 0$.

To investigate the kinetic model a numerical approach is often needed, due to the high dimensional partial differential equations. The numerical description can be seperated into a local (flux-tube) and global description. Both have their numerical problems concerning the plasma beta β parameter. For local gyrokinetic simulations a high plasma beta results in a saturation of the heat fluxes at a high level of transport, which is known as the nonzonal transition (NZT) and was not found in realistic experiments. This behaviour limits in flux-tube simulations the plasma beta under the critical value for MHD stability. The global electromagnetic gyrokinetic simulations mainly suffer from the *cancellation problem*[3] examined in codes which use the particle-in-cell or the Eulerian methods[5]. Here, the cancellation problem scales with the quotient $\beta/k_\perp^2$ [15], which again limits investigations to very low plasma beta and long perpendicular turbulent length scales linked to the wavevector $k_\perp$. Overall, these problems limit the electromagnetic investigations to extremely low plasma beta. To mitigate the cancellation problem a new technique was found in global nonlinear gyrokinetc simulations. This technique introduces an additional field equation through Faraday's law, the *plasma induction*[4 11]
Now one would ask:

Is it possible to mitigate the cancellation problem in local gyrokinetic simulations with the introduction of the plasma induction?

The goal of this thesis is to lay the groundwork for the global electromagnetic gyrokinetic model for GKW and to mitigate the cancellation problem in the local version of GKW.

For that purpose, the field equation for the plasma induction is implemented by using Faraday's law into GKW. The overall scheme of this thesis follows Chapter 5 of the Dissertation of Paul Charles Crandall[4].

CHAPTER

2

Plasma Physics Basics

First, it is necessary to discuss the plasma pyhics basics at the beginn of this thesis. For this the motion of charged particle and the relevance of the plasma beta β will be discussed. This chapter is based on the introduction book to Tokamaks from John Wesson[25] For more books regarding plasma physics basics the reader is referred to

- Kaufmann, Michael 2013 *Plasmaphysik und Fusionsforschung*. Wiesbaden: Springer Fachmedien Wiesbaden
- Stroth, Ulrich 2018 *Plasmaphysik: Phänomene, Grundlagen und Anwendungen*. Berlin, Heidelberg: Springer Berlin Heidelberg.

2.1 Charged Particle Motion

In magnetic confinement devices like the Tokamak reactor, the charged particles experience forces caused by magnetic and electric fields which result in distinct motion under the associated force. Charged particles can be separated in species, e.g. electrons and ions, which will be later on indicated by the index "s" in the governing equations in Chapter 3.8 if needed. Until then the index will be dropped for simplicity.

2.1.1 Motion in Electromagnetic Fields

Due to the Lorentz force, particles with a velocity $v_\perp$ perpendicular to the homogenous magnetic field, undergo a circular motion in the plane perpendicular to the magnetic field [Fig. 2.1(a)]. This type of motion has circular frequency, which is often referred to as *cyclotron frequency* and is defined as

$$\omega_\mathrm{c} = \frac{|q|B}{m} \ , \tag{2.1}$$

where m and q are the mass and the charge of the particle and B the strength of the magnetic field. The radius, the so called *Larmor radius*, of this motion is given by

$$\rho = \frac{mv_\perp}{|q|B} \tag{2.2}$$

with the center often being referred to as *guiding center*. Note that since the Lorentz force depends on the species charge of the particle, the circulation direction is the opposite between electrons in ions. Due to Coulomb collisions the plasma gets thermalized. Together with the Maxwell-Boltzmann distribution the typical thermal velocity is

$$v_\mathrm{th} = \sqrt{\frac{2T}{m}} \ , \tag{2.3}$$

where T represents the species temperature. Based on the thermal velocity v_th the *thermal Larmor radius* gets introduced as

$$\rho_\mathrm{th} = \frac{mv_\mathrm{th}}{|q|B} \ . \tag{2.4}$$

In the absence of forces in the direction parallel to the magnetic field the particles can move freely in parallel direction to the homogenous magnetic field. The velocity of this motion is in the order of the thermal velocity v_th and is dominated by electrons due to their lighter mass compared to ions ($v_\mathrm{th,e}/v_\mathrm{th,i} = 60$). When an electric field $E_\parallel$ with a

component parallel to the magnetic field influences the plasma, the charged particles are accelerated by the electric force

$$F_{\parallel,E} = qE_{\parallel} \ . \tag{2.5}$$

The parallel motion derives from the equation of motion. Here the direction of the motion also depends on the species type [Fig. 2.1(b)].

Since magnetic fields are not always homogenous, an inhomogeneous magnetic field with its gradient ∇B containing a component parallel to the magnetic field which is given by

$$\nabla_{\parallel} B = \frac{\mathbf{B}}{B} \cdot \nabla B \tag{2.6}$$

causes the force

$$F_{\parallel,\nabla_{\parallel}B} = -\frac{mv_{\perp}^2}{2B}\nabla_{\parallel}B = -\mu\nabla_{\parallel}B \ ; \qquad \mu = \frac{mv_{\perp}^2}{2B} \tag{2.7}$$

with *magnetic moment* μ. The magnetic moment μ is an adabatic invariant (constant of motion) if the variation of the magnetic field over time is smaller than the inverse of the cyclotron frequency ω_c^{-1} and the spatial variation is larger than Larmor radius ρ. Note that, the force is not dependant on the charge q, so the direction of the force $F_{\parallel,\nabla_{\parallel}B}$ is the same for electrons and ions. The resulting force has its application in the mirror effect where a charged particle gets reflected due to this force [Fig. 2.1(c)].

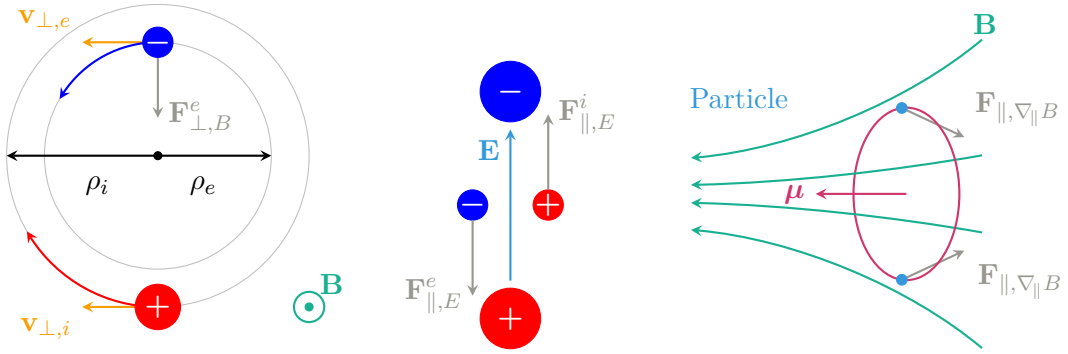

Figure 2.1: Forces acting on a charged particle:
(a) Circular motion caused by Lorentz force $\mathbf{F}^s_{\perp,B}$ with perpendicular velocity $\mathbf{v}_{\perp,s}$ and Larmor radius ρ_s,
(b) Electric force $\mathbf{F}^s_{\parallel,E}$ with electric field $\mathbf{E}$,
(c) Mirror effect with force $\mathbf{F}_{\parallel,\nabla_{\parallel}B}$ and magnetic moment μ caused by an inhomogeneous magnetic field $\mathbf{B}$.

2.1.2 Drifts in the Guiding Center

In the presence of a magnetic field (homogenous, inhomogeneous or perturbed) and electric fields the guiding center undergoes slow (compared to the thermal velocity v_{th}) drift motions perpendicular to the magnetic field. There are several examples for this drift motion. Here the main three drift types will be covered in the following.

1. **E × B Drift:**
   If an electric field **E** with a perpendicular component together with the magnetic field **B** (both fields are homogenous) is present the acting Coulomb force and Lorentz force result into a drift of the guiding center with

   $$\mathbf{v}_E = \frac{\mathbf{E} \times \mathbf{B}}{B^2} \tag{2.8}$$

   which is called the E × B drift. Since the direction of both acting forces depends on the species type the E × B drift is the same for every species [Fig. 2.2(a)].

2. **∇B Drift:**
   An inhomogeneous magnetic field causes a gradient ∇B of the magnetic field. Because of that gradient the guiding center undergoes a ∇B drift defined by

   $$\mathbf{v}_{\nabla B} = \frac{m v_\perp^2}{2q} \frac{\mathbf{B} \times \nabla B}{B^3} \ . \tag{2.9}$$

   The direction of the ∇B drift depends on the species type [Fig. 2.2(b)].

3. **Curvature Drift:**
   Due to centrifugal force acting on the particle in a curved magnetic field the guiding center experiences a curvature drift according to

   $$\mathbf{v}_C = \frac{m v_\parallel^2}{q} \frac{\mathbf{B} \times \mathbf{C}}{B^2} = \frac{m v_\parallel^2}{q} \frac{\mathbf{B} \times \nabla B}{B^3} \ ; \qquad \mathbf{C} = -(\mathbf{b} \cdot \nabla)\mathbf{b} = \frac{\nabla B}{B} \ , \tag{2.10}$$

   where **b** is the unit vector along the magnetic field. To obtain the result for the curvature **C** in Eq. (2.10) the plasma pressure has to be small compared to the magnetic field strength B. In the form of Eq. (2.10) ∇B and curvature drift can be treated similarly.

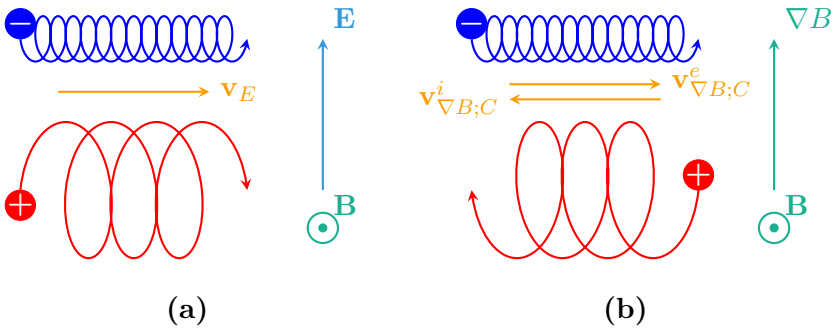

Figure 2.2: Dirft motion in gyrocenter:

(a) E × B Drift with drift velocity $\mathbf{v}_E$, electric field **E** and magnetic field **B**,

(b) ∇B Drift/Curvature Drift with drift velocity $\mathbf{v}^s_{\nabla B;C}$, magnetic field **B** and gradient of the magnetic field ∇B.

2.2 Magnetic Confinement and Plasma Rotation

In Tokamak devices strong magnetic fields confine the hot plasma. As mentioned in Chapter 2.1 a magnetic field forces a perpendicular particle motion and a motion which contains the gyro motion and slow perpendicular guiding center drifts. Because of the much smaller size of the Larmor radius compared to the device size R the particle and energy losses are caused by the guiding center drifts. To avoid additional loss of particles because of the parallel motion, the field lines of the magnetic field in the Tokamak devices is shaped like a torus. This type of geometry has nested surfaces with constant magnetic flux, the so-called *flux surfaces*, and magnetic field lines which lie on these surfaces. To maintain stability the magnetic field has a toroidal and a poloidal component. According to the force balance the magnetic field is equivalent to the plasma pressure which means that on flux-surfaces the plasma pressure is constant.[22,25] The toroidal component is produced by external coils whereas the poloidal component is provided by the toroidal plasma current. Together the components result in a magnetic field which follows helical trajectories [Fig 2.3]. To characterize the quality of confinement the so-called *plasma beta* is used and is given as

$$\beta = \frac{nT}{B^2/2\mu_0} \ , \tag{2.11}$$

with n the plasma density, T as temperature, μ_0 the permeability in vacuum and the magnetic field strength B. Respectively, the plasma beta compares the thermal plasma pressure nT to the ambient magnetic field pressure $B^2/2\mu_0$. For fusion devices the plasma beta has to be a bit smaller than 1 ($\beta < 1$) for optimal confinement. In a Tokamak reactor the plasma beta has a typical order of a few percent. The plasma beta is also considered to be one of the fundamental dimensionless parameters in plasma physics, due to its relevance for the outcome, the fusion rate ($\sim \beta^2$), bootstrap fraction ($\sim \beta$) and MHD stability of a fusion device. Furthermore, the plasma beta is an indicator for the relevance of electromagnetic effects in a gyrokinetic systems, since electromagentic fields vanish in the limit $\beta \to 0$.[4]

The rotation of the plasma can be described in a co-rotating frame of reference, which is rigidly rotating with the velocity $\mathbf{u}_0$ and will be used later on in the derivation of the gyrokinetic equations in Chapter 3.2. It assumens that the poloidal component of the plasma rotation is much smaller compared to the toroidal component and will be neglected. With this assumption in mind the reference frame is chosen to move in the toroidal direction exclusivly and its velocity $\mathbf{u}_0$ can be expressed as

$$\mathbf{u}_0 = \mathbf{\Omega} \times \mathbf{x} = R^2 \Omega \nabla \varphi \ , \tag{2.12}$$

where $\mathbf{\Omega}$ is the constant angular frequency, φ is the toroidal angle and $R\nabla\varphi$ is the unit vector in the toroidal direction.

Since the rotation of the plasma in the labortory frame is not a rigid body rotation, it will be characterized by the radial profile of the angular velocity $\hat{\Omega}(\psi)$. The angular frequency of the rotating frame Ω is chosen to match the plasma rotation on a certain point, i.e. $\Omega = \hat{\Omega}(\psi_r)$. The plasma rotation in the co-rotating frame of reference will be denoted as

$$\omega_\varphi(\psi) = \hat{\Omega}(\psi) - \Omega. \tag{2.13}$$

with the rotation speed along the magnetic field line

$$u_\parallel = \frac{RB_\mathrm{t}}{B}\omega_\varphi(\psi)\ , \tag{2.14}$$

where B_t is the toroidal component of the magnetic field.[19]

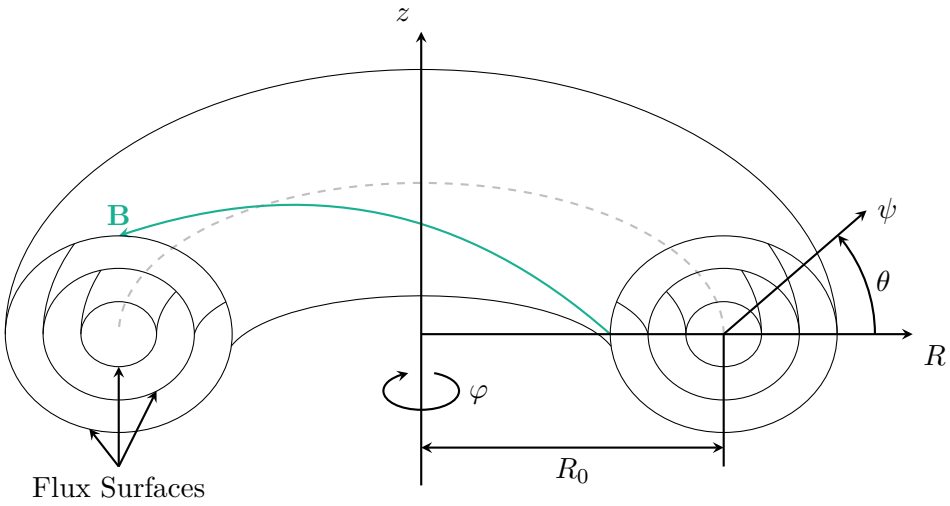

Figure 2.3: Toroidal flux surfaces in Tokamak plasma with helical magnetic field (green line) in torus coordinates (ψ (radial), φ (toroidal), θ (poloidal)) or cylindrical coordinates (z, R, $-\varphi$).[1]

CHAPTER

3

The Gyrokinetic Theory

In this chapter the following scheme will be discussed:

1. The Lagrangian L for a particle in a electromagnetic field is reformulated in the fundamental one-form γ according to

$$\int \mathrm{d}t\ L = \int \gamma\ . \tag{3.1}$$

   From this point on the fundamental one-form and Lagrangian referes to the quantity γ. Then, the Lagrangian γ will be transformed in the guiding center phase space and separated in its equilibrium and perturbated part. Through the Lie transformation the Lagrangian gets transformed into the gyrocenter phase space by eliminating the gyro phase.

2. Plugging the Lagrangian into the Euler-Lagrangian equation yields the equations of motions. From the equations of motion the Vlasov equation can be derived.

3. The Vlasov equation solves for the density distribution function, which will be used to express the particle density n and current $\mathbf{j}$ with the moments of the distribution function.

4. Particle density n and current $\mathbf{j}$ will then be plugged into the Maxwell's equations, i.e. the field equations.

5. The cancellation problem will be discussed and the mitigation technique will be introduced for GKW.

This chapter is based on the Dissertation of Tilman Dannert[6] and the derivation document provided by the GKW group[23]. The derivation of Faraday's law in Chapter 3.8.5 is based on the disseration of Paul Crandall[4].

3.1 Gyrokinetic Ordering

In the derivation of the gyrokinetic theory the aim is to decouple the effect of small scale, small amplitude fluctuations of the plasma in the Langrangian. For that, the properties of fluctuations will be chosen as small parameter, which will result in the ordering assumptions applied in gyrokinetic theory. This section is based on Ref. 2, 23 and 13. There are the following assumptions:

- **Low Frequency**
  The characteristic fluctuation frequency is small compared to the cyclotron frequency
  $$\Rightarrow \frac{\omega}{\omega_\mathrm{c}} \ll 1 \ .$$
- **Anisotropy**
  The length scales of the turbulence are associated with the wave vector $\mathbf{k}$ which can be seperated into a perpendicular component $k_\perp = |\mathbf{k} \times \mathbf{b}|$ and a parallel component $k_\parallel = |\mathbf{k} \cdot \mathbf{b}|$ where $\mathbf{b}$ is parallel to the toroidal component of the magnetic field. The perpendicular correlation length of the turbulence has a length scale of around $10 - 100$ gyroradii while the parallel length scales can be of the order of meters, which can be expressed in wavenumber as
  $$\Rightarrow \frac{k_\parallel}{k_\perp} \ll 1 \ .$$
- **Strong Magnetization**
  The Larmor radius ρ is small compared to the gradient length scales for
  - Background Density: $L_n = n_0 \left(\frac{\mathrm{d}n_0}{\mathrm{d}x}\right)^{-1}$
  - Background Temperature: $L_T = T_0 \left(\frac{\mathrm{d}T_0}{\mathrm{d}x}\right)^{-1}$
  - Background Magnetic Field: $L_B = B_0 \left(\frac{\mathrm{d}B_0}{\mathrm{d}x}\right)^{-1}$

  $$\Rightarrow \frac{\rho}{L_n} \sim \frac{\rho}{L_T} \sim \frac{\rho}{L_B} \ll 1 \ .$$
- **Small Fluctuations**
  The fluctuating part of the gyrocenter distribution function F_1 is assumend to be small compared to the background distribution function F_0
  $$\Rightarrow \frac{F_1}{F_0} \ll 1 \ .$$
  Furthermore, the fluctuations of the vector potential $\mathbf{A}_1$ and scalar potentials Φ_1 are small compared to there background part
  $$\Rightarrow \frac{\mathbf{A}_1}{\mathbf{A}_0} \sim \frac{\Phi_1}{\Phi_0} \ll 1 \ .$$

Together these assumptions lead to the gyrokinetic ordering

$$\frac{\omega}{\omega_{\mathrm{c}}} \sim \frac{k_{\parallel}}{k_{\perp}} \sim \frac{\rho}{L_n} \sim \frac{\rho}{L_T} \sim \frac{\rho}{L_B} \sim \frac{F_1}{F_0} \sim \frac{\mathbf{A}_1}{\mathbf{A}_0} \sim \frac{\Phi_1}{\Phi_0} \sim \epsilon_\delta \ , \tag{3.2}$$

where ϵ_δ is a small parameter. For the derivation of the gyrokinetic equations of GKW all derived equations are evaluated up to the first order of the ratio of the reference thermal Larmor radius $\rho_{\mathrm{th,ref}}$ and the equilibrium magnetic length scale L_B as small parameter and is defined as

$$\rho_\star = \frac{\rho_{\mathrm{th,ref}}}{L_B} = \frac{m_{\mathrm{ref}} v_{\mathrm{th,ref}}}{e B_{\mathrm{ref}}} \sim \epsilon_\delta \ . \tag{3.3}$$

3.2 Gyrokinetic Lagrangian

3.2.1 Lagrangian in Patricle Phase Space

The Lagrangian of a particle γ with mass m and charge number Z in the electro magnetic field will be described through the particle position $\mathbf{x}$ and the velocity $\mathbf{v}$ as coordinates $\{\mathbf{x}, \mathbf{v}\}$ and can be written as

$$\gamma = \gamma_\nu \mathrm{d}z^\nu = \underbrace{(m\mathbf{v} + Ze\mathbf{A}(\mathbf{x}))}_{\text{Sympletic Part}} \cdot \mathrm{d}\mathbf{x} - \underbrace{\left(\frac{1}{2}mv^2 + Ze\Phi(\mathbf{x})\right)}_{\text{Hamiltonian } H(\mathbf{x},\mathbf{v})} \mathrm{d}t \ , \tag{3.4}$$

where $\mathbf{A}$ and Φ are the vector and scalar potential, ν indexes the six coordinates and Einstein notation is applied.

The defined Lagrangian γ will then be transformed in the rotating frame of reference [Ch. 2.2], which can be achieved through the following Lorentz transformation

$$\mathbf{v} \to \mathbf{v} + \mathbf{u}_0 \qquad \mathbf{E} \to \mathbf{E} + \mathbf{u}_0 \times \mathbf{B} \qquad \Phi \to \Phi + \mathbf{A} \cdot \mathbf{u}_0 \ . \tag{3.5}$$

After performing the transformation outlined in Ref. 19 the Lagrangian γ becomes

$$\gamma = (m\mathbf{v} + m\mathbf{u}_0 + Ze\mathbf{A}(\mathbf{x})) \cdot \mathrm{d}\mathbf{x} - \left(\frac{1}{2}mv^2 - \frac{1}{2}mu_0^2 + Ze\Phi(\mathbf{x})\right) \mathrm{d}t \ . \tag{3.6}$$

In the next step small scale perturbations of the electromagnetic field are introduced as following

$$\Phi = \Phi_0 + \Phi_1 \qquad \mathbf{A} = \mathbf{A}_0 + \mathbf{A}_1 \ . \tag{3.7}$$

Here, it is assumend that the equilibrium electric field is zero in a stationary plasma, but it will be kept in case of finite plasma rotation. According to the gyrokinetic ordering [Ch. 3.1] the perturbations are in the first order of $\rho_\star$. Taking everything into account the Lagrangian in the particle phase space with perturbations can be written as

$$\begin{aligned} \gamma &= \gamma_0 + \gamma_1 \\ \gamma_0 &= (m\mathbf{v} + m\mathbf{u}_0 + Ze\mathbf{A}_0(\mathbf{x})) \cdot \mathrm{d}\mathbf{x} - \left(\frac{1}{2}mv^2 - \frac{1}{2}mu_0^2 + Ze\Phi_0(\mathbf{x})\right) \mathrm{d}t \\ \gamma_1 &= Ze\mathbf{A}_1(\mathbf{x}) \cdot \mathrm{d}\mathbf{x} - Ze\Phi_1(\mathbf{x}) \, \mathrm{d}t \ . \end{aligned} \tag{3.8}$$

3.2.2 Lagrangian in Guiding Center Phase Space

For the description of charged particle behaviour in the Tokamak device the *guiding center coordinates* are used [Fig. 3.1]. This set of coordinates are defined as the following

$$\begin{aligned} \mathbf{X}(\mathbf{x},\mathbf{v}) &= \mathbf{x} - \mathbf{r} & v_\parallel &= \mathbf{v}\cdot\mathbf{b}(\mathbf{x}) \\ \mu(\mathbf{x},\mathbf{v}) &= \frac{m v_\perp^2(\mathbf{x})}{2B(\mathbf{x})} & \theta(\mathbf{x},\mathbf{v}) &= \arccos\left(\frac{1}{v_\perp}\left(\mathbf{b}(\mathbf{x})\times\mathbf{v}\right)\cdot\hat{\mathbf{e}}_1\right) \ , \end{aligned} \tag{3.9}$$

where the guiding center follows the magnetic field with the parallel velocity $v_\parallel$. The gyromotion is described together with the magnetic moment μ, the guiding center $\mathbf{X}$ and the gyro phase θ which gives a parameter set of six quantities $\{\mathbf{X}, v_\parallel, \mu, \theta\}$. Vector $\mathbf{b}(\mathbf{x})$ is the unit vector in the direction of the equilibrium magnetic field and $\mathbf{r} = \rho(\mathbf{x},\mathbf{v})\mathbf{a}(\mathbf{x},\mathbf{v})$ is the vector pointing from the guiding center to the particles postion, which is defined by the unit vector $\mathbf{a}(\mathbf{x},\mathbf{v})$ and its length is the Lamor radius $\rho(\mathbf{x},\mathbf{v})$. The unit vector $\mathbf{a}(\mathbf{x},\mathbf{v})$ can be expressed in a local orthonormal basis as the function of the gyroangle θ

$$\mathbf{a}(\theta) = \hat{\mathbf{e}}_1\cos\theta + \hat{\mathbf{e}}_2\sin\theta \ . \tag{3.10}$$

The vectors $\mathbf{b}$, $\hat{\mathbf{e}}_1$ and $\hat{\mathbf{e}}_2$ form a local Cartesian coordinate system at the guiding center position.

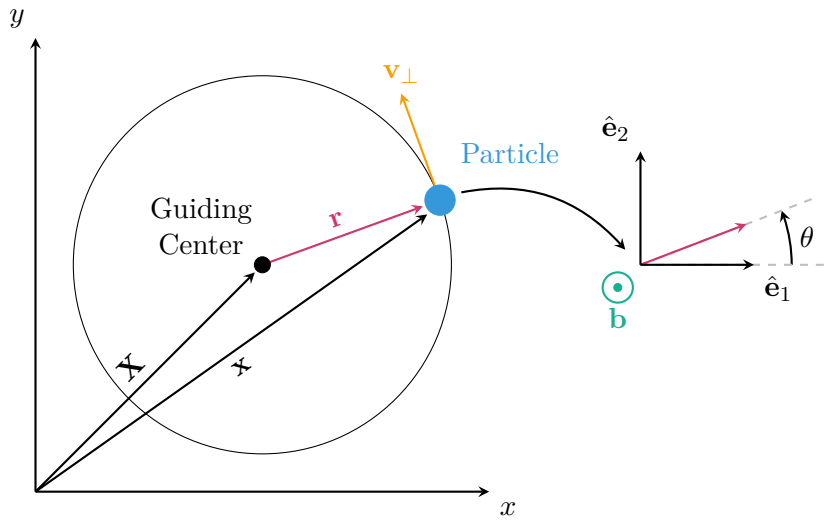

Figure 3.1: Sketch of guiding center coordinates where the charged particle performs a circular motion around the guiding center.[10]

To transform the lagrangian into the guiding center coordinates the following relation will be used

$$\Gamma_\eta = \gamma_\nu \frac{\mathrm{d}z^\nu}{\mathrm{d}Z^\eta} \ , \tag{3.11}$$

where Γ_η is a component of the guiding center Lagrangian. To calculate the new coordinates the transformation [Eq. (3.9)] has to be inverted to provide the old coordinates as a function of the new one $z(Z)$. Here, the direct transformation is uniquely determined if the magnetic field is known at the particle postion $\mathbf{x}$. However, the inverse transformation is not uniquely due to the dependence of the Larmor radius ρ on magnetic field at the particle position $\mathbf{x}$. Applying Taylor expansion around the guiding center $\mathbf{X}$ for the Larmor radius ρ yields $\rho(\mathbf{x}) \approx \rho(\mathbf{X})$. Note, that terms of order ρ^2, which lead to second order terms in $\rho_\star$, will be neglected due to the gyrokinetic ordering. The Taylor expansion results in the particle position $\mathbf{x}$ being expressed with the guiding center coordinates as

$$\mathbf{x}(\mathbf{X}, \theta) \approx \mathbf{X} + \rho(\mathbf{X})\mathbf{a}(\theta) \ . \tag{3.12}$$

The particle velocity $\mathbf{v}$ is the sum of the velocity along the magnetic field $v_\parallel$, the gyration velocity $\mathbf{v}_\perp$ and the drift velocity, which will be neglected since the particle drifts can be described by the motion of the guiding center. To summarize the velocity $\mathbf{v}$ in the guiding center frame can be expressed as

$$\mathbf{v} = v_\parallel \mathbf{b}(\mathbf{x}) + \mathbf{v}_\perp = v_\parallel \mathbf{b}(\mathbf{x}) + \rho(\mathbf{x})\dot{\mathbf{a}}(\theta) \ . \tag{3.13}$$

Applying Taylor expansion around the guiding center $\mathbf{X}$ results in the following expression

$$\mathbf{v}(\mathbf{X}, v_\parallel, \mu, \theta) \approx v_\parallel \left[\mathbf{b}(\mathbf{X}) + \partial_{\mathbf{X}} \mathbf{b}(\mathbf{X}) \cdot \mathbf{a}(\theta)\rho(\mathbf{X}, \mu)\right] + \rho(\mathbf{X}, \mu)\dot{\mathbf{a}}(\theta) \ . \tag{3.14}$$

Now, the transformation [Eq. (3.11)] can be applied to express the Lagrangian in the new coordinates. For that the components of the Lagrangian of the particle phase space γ_ν and the equation for $\mathbf{v}$ in guiding center coordinates [Eq. (3.14)] will be inserted. After that, the gyroaveraging operator $\mathcal{G}$ will be used, which is defined as the integral over the gyrophase θ

$$\mathcal{G}\{G(\mathbf{x})\} = \bar{G}(\mathbf{X}) = \frac{1}{2\pi} \int_0^{2\pi} \mathrm{d}\theta \ G(\mathbf{X} + \mathbf{r}(\theta)) \ , \tag{3.15}$$

with an example field $G(\mathbf{x})$. Due to the definition of the vector $\mathbf{a}$ [Eq. (3.10)] the first order terms in $\mathbf{a}$ and $\dot{\mathbf{a}}$ disappear under gyroaveraging. Following all the previous steps, the Lagrangian in guiding center coordinates merges

$$\begin{aligned} \bar{\Gamma} = &\left(m v_\parallel \mathbf{b}(\mathbf{X}) + m\mathbf{u}_0 + Ze\mathbf{A}(\mathbf{X})\right) \cdot \mathrm{d}\mathbf{X} + \frac{2\mu m}{Ze}\mathrm{d}\theta \\ &- \left(\frac{1}{2} m v_\parallel^2 - \frac{1}{2} m u_0^2 + Ze\Phi(\mathbf{X}) + \mu B(\mathbf{X})\right) \mathrm{d}t \ . \end{aligned} \tag{3.16}$$

Note that as a consequence of the Lagrangian being independent of the gyrophase θ, the magnetic moment μ (the associated conjugated coordinate pair of θ) becomes an invariant of the motion ($\dot{\mu} = 0$).

As in Chapter 3.2.1 perturbations [Eq. (3.7)] will get introduced to the guiding center Lagrangian. The transformation of the equilibrium part was performed above, so only the perturbation part with the perturbated Lagrangian in the particle phase space γ_1 has to be transformed to the guiding center phase space. The transformation is analogous to the calculations before, the key difference being that fluctuation quantities vary on a small length scale and Taylor expansion around the guiding center $\mathbf{X}$ can not be applied advantageous. After inserting the components of the perturbated Lagrangian γ_1 into the transformation [Eq. (3.11)] and neglecting terms of order ρ^2, due to gyrokinetic ordering, the fundamental one form in the guiding center coordinates can be expressed as

$$\begin{aligned}
\Gamma &= \bar{\Gamma}_0 + \Gamma_1 \\
\bar{\Gamma}_0 &= \left(mv_\parallel \mathbf{b}(\mathbf{X}) + m\mathbf{u}_0 + Ze\mathbf{A}_0(\mathbf{X})\right) \cdot \mathrm{d}\mathbf{X} + \frac{2\mu m}{Ze}\mathrm{d}\theta \\
&\quad - \left(\frac{1}{2}mv_\parallel^2 - \frac{1}{2}mu_0^2 + Ze\Phi_0(\mathbf{X}) + \mu B_0(\mathbf{X})\right)\mathrm{d}t \\
\Gamma_1 &= Ze\mathbf{A}_1(\mathbf{x}) \cdot \mathrm{d}\mathbf{X} + \frac{Z}{|Z|}\frac{1}{v_\perp}\mathbf{A}_1(\mathbf{x}) \cdot \mathbf{a}(\theta)\mathrm{d}\mu + \frac{Z}{|Z|}\frac{2\mu}{v_\perp}\mathbf{A}_1(\mathbf{x}) \cdot \frac{\mathrm{d}\mathbf{a}(\theta)}{\mathrm{d}\theta}\mathrm{d}\theta - Ze\Phi_1(\mathbf{x})\mathrm{d}t \ .
\end{aligned} \tag{3.17}$$

3.2.3 Lagrangian in Gyrocenter Phase Space

The transformation of the guiding center Lagrangian Γ into the Lagrangian in gyrocenter phase space $\bar{\Gamma}$ aims to remove the gyroangle θ dependence introduced by the fluctuations of the guiding center lagrangian. To destinguish between the guiding center and the gyrocenter coordinates all quantities associated with the gyrocenter are getting an overbar, i.e. $\bar{\Gamma}$. The new set of gyrocenter coordinates are given by $\{\bar{\mathbf{X}}, \bar{v}_\parallel, \bar{\mu}\}$. Since the derivation of the lagrangian in the gyrocenter phase space $\bar{\Gamma}$ uses the Lie transform perturbation method, which is beyond the scope of this thesis, the reader is referred to the Refs. 6 and 23 for more details. The Lagrangian in the gyrocenter phase space can be expressed as

$$\begin{aligned}\bar{\Gamma} &= \bar{\Gamma}_0 + \bar{\Gamma}_1 \\ &= \left(mv_\parallel \mathbf{b}_0(\mathbf{X}) + m\mathbf{u}_0 + Ze\left(\mathbf{A}_0(\mathbf{X}) + \bar{\mathbf{A}}_1(\mathbf{X})\right)\right)\cdot \mathrm{d}\mathbf{X} + \frac{2\mu m}{Ze}\mathrm{d}\theta \\ &\quad - \left(\frac{1}{2}m\left(v_\parallel^2 - u_0^2\right) + Ze\left(\Phi_0(\mathbf{X}) + \bar{\Phi}_1(\mathbf{X})\right) + \mu\left(B_0(\mathbf{X}) + \bar{B}_{1\parallel}(\mathbf{X})\right)\right)\,\mathrm{d}t\ ,\end{aligned} \tag{3.18}$$

where B_0 is the equilibrium magnetic field and $\bar{B}_{1\parallel}$ is the magnetic field introduced by the vector potential $\mathbf{A}_1$. Note, that the perturbations of the scalar and vector potential will be seperated into an oscillating and a gyroaveraged part which will be expressed as

$$\Phi_1 = \widetilde{\Phi}_1 + \bar{\Phi}_1 \qquad \mathbf{A}_1 = \widetilde{\mathbf{A}}_1 + \bar{\mathbf{A}}_1\ , \tag{3.19}$$

although the oscillating parts will be added to the gauge function of the Lie transformation and will not be included in the Lagrangian of the gyrocenter phase space. The quantity $\bar{B}_{1\parallel}$ is the shorter notation of following gyroaveraged quantity defined as

$$\mathcal{G}\{Ze\mathbf{A}_1(\mathbf{x})\cdot\mathbf{v}_\perp(\mathbf{X},\mu,\theta)\} = \mu\bar{B}_{1\parallel}(\mathbf{X})\ . \tag{3.20}$$

3.3 Gyrokinetic Equation

3.3.1 Vlasov Equation

Because of the large number of particles in the fusion plasma a prediction on the basis of Newton-Maxwell dynamics cannot be achieved in simulation, but this problem can be solved with a statistical approach. Therefore, the distribution function $f(\mathbf{x}, \mathbf{v}, t)$ in the particle phase space $\{\mathbf{x},\ \mathbf{v}\}$ will be considered. Because collisions occur at much smaller frequencies than the characteristic frequencies connected to turbulence, the collisionless model is often preferred[7] which results through evolution of the particle density distribution function in the *Vlasov equation*

$$\frac{\partial f}{\partial t} + \dot{\mathbf{x}} \cdot \frac{\partial f}{\partial \mathbf{x}} + \dot{\mathbf{v}} \cdot \frac{\partial f}{\partial \mathbf{v}} = 0 \ . \tag{3.21}$$

In the gyrocenter phase space $\{\mathbf{X}, v_\parallel, \mu\}$, the overbar introduced in Chapter 3.2.3 gets droped for simplicity for all quantities, the Vlasov equation with the gyrocenter distribution function F takes the following form

$$\frac{\partial F}{\partial t} + \dot{\mathbf{X}} \cdot \frac{\partial F}{\partial \mathbf{X}} + \dot{v}_\parallel \cdot \frac{\partial F}{\partial v_\parallel} = 0 \ , \tag{3.22}$$

where the gyrophase θ is still an ignorable coordinate and the time derivative of the magnetic moment μ is zero, because the magnetic moment μ is an exact invariant. In Equation (3.22) the terms of the time derivative of the gyrocenter $\dot{\mathbf{X}}$ and the parallel velocity $\dot{v_\parallel}$ have to be expressed through the gyrocenter Lagrangian with the Euler-Lagrange equation. The Euler-Lagrange equation can be written as

$$\left(\frac{\partial \gamma_j}{\partial z^i} - \frac{\partial \gamma_i}{\partial z^j}\right) \frac{\mathrm{d}z^j}{\mathrm{d}t} = \frac{\partial H}{\partial z^i} + \frac{\partial \gamma_i}{\partial t} \ . \tag{3.23}$$

Inserting Equation (3.18) into the Euler-Lagrange equation and applying multiple calculations detailed in Ref. 23 the equations of motion can be obtained as

$$\begin{aligned} \dot{\mathbf{X}} &= \mathbf{b}_0 v_\parallel + \mathbf{v}_\chi + \mathbf{v}_\mathrm{D} \qquad & \dot{v}_\parallel &= \frac{\dot{\mathbf{X}}}{m v_\parallel} \cdot \Big(Ze\bar{\mathbf{E}} - \mu \nabla (B_0 + \bar{B}_{1\parallel}) + \underbrace{\frac{1}{2} m \nabla u_0^2}_{mR\Omega^2 \nabla R} \Big) \\ \dot{\mu} &= 0 & \dot{\theta} &= \omega_\mathrm{c} - \frac{Ze}{m} \partial_\mu \left(Ze\bar{\mathbf{A}}_1 \cdot \dot{\mathbf{X}} - Ze\bar{\Phi}_1 - \mu \bar{B}_{1\parallel} \right) \ , \end{aligned} \tag{3.24}$$

with the drift velocity $\mathbf{v}_\chi$ defined as the sum of the streaming velocity perpendicular to the perturbated magnetic field $\mathbf{v}_{\bar{B}_{1\perp}}$, the $\mathrm{E} \times \mathrm{B}$ drift in the total electric field $\mathbf{v}_{\bar{E}}$ and the grad-B dirft of the parallel perturbed magnetic field $\mathbf{v}_{\nabla \bar{B}_{1\parallel}}$. The drift velocity

$\mathbf{v}_{\mathrm{D}}$ containing the sum of the curvature drift $\mathbf{v}_C$, the grad-B drift of the equilibrium magnetic field $\mathbf{v}_{\nabla B_0}$ and the drifts due to the Coriolis force $\mathbf{v}_{\mathrm{Co}}$ and centrifugal force $\mathbf{v}_{\mathrm{Ce}}$. Note that, the term containing u_0^2 got replaced with $u_0^2 = R^2\Omega^2$ from Equation (2.12). The quantity χ can be expressed as

$$\chi = \underbrace{(\Phi_0 + \bar{\Phi}_1)}_{\bar{\Phi}} - v_\parallel \bar{A}_{1\parallel} + \frac{\mu}{Ze}\bar{B}_{1\parallel} \tag{3.25}$$

which defines the drift velocity $\mathbf{v}_\chi$

$$\mathbf{v}_\chi = \frac{\mathbf{b}_0 \times \nabla\chi}{B_0} = \mathbf{v}_{\bar{E}} + \mathbf{v}_{\bar{B}_{1\perp}} + \mathbf{v}_{\nabla\bar{B}_{1\parallel}} \ , \tag{3.26}$$

with $\mathbf{b}_0 \times (\nabla A_{1\parallel}) \approx \nabla \times (A_{1\parallel}\mathbf{b}_0) = \mathbf{B}_{1\perp}$. The total electric field $\bar{\mathbf{E}}$ is defined as

$$\bar{\mathbf{E}} = -\nabla\bar{\Phi} - \partial_t \bar{\mathbf{A}}_1 = -\nabla\bar{\Phi} - \partial_t \left(\mathbf{b}_0 \cdot \bar{A}_{1\parallel} + \bar{\mathbf{A}}_{1\perp}\right) \ . \tag{3.27}$$

Due to normalization assumptions in gyrokinetics[17] the time derivative of the vector potential $\partial_t \bar{\mathbf{A}}_1$ is one order smaller tham the gradient of the electrostatic potential $\nabla\bar{\Phi}$ and the contribution of the vector potential will be neglected in the $\mathbf{v}_{\bar{E}}$ velocity term.

3.3.2 The delta-*f* Approximation

The delta-*f* approximation separates the density distribution function F into an equilibrium part F_0 and perturbation part F_1, i.e. $F = F_0 + F_1$. Applying the delta-*f* approximation on the gyrocenter Vlasov equation leads to

$$\frac{\partial F_1}{\partial t} + \dot{\mathbf{X}} \cdot \nabla F_1 + \dot{v}_\parallel \cdot \frac{\partial F_1}{\partial v_\parallel} = \underbrace{-\dot{\mathbf{X}} \cdot \nabla F_0 - \dot{v}_\parallel \frac{\partial F_0}{\partial v_\parallel}}_{S} , \tag{3.28}$$

with the source term S. Substituting the equations for $\dot{\mathbf{X}}$ and $\dot{v}_\parallel$ from Equation (3.24)into the delta-*f* approximated Vlasov equation results in

$$\frac{\partial F_1}{\partial t} + \dot{\mathbf{X}} \cdot \nabla F_1 - \frac{\mathbf{b}_0}{m} \cdot \left(Ze\nabla\Phi_0 + \mu\nabla B_0 - mR\Omega^2\nabla R \right) \cdot \frac{\partial F_1}{\partial v_\parallel} = S \, . \tag{3.29}$$

Note that only the terms of order $\rho_\star$ has to be kept in $\dot{v}_\parallel \partial_{v_\parallel} F_1$, which results in neglecting the drift velocities $\mathbf{v}_\chi$ and $\mathbf{v}_\mathrm{D}$ and the contribution of $\bar{B}_{1\parallel}$ and $\bar{\Phi}_1$, since these terms are after calculation of order $\rho_\star^2$.

The equilibrium distribution function F_0 is assumed to be a Maxwellian which includes a finite equilibrium electric field Φ_0 to balance the centrifugal force (in the co-rotating frame) due to toroidal rotation of the plasma.
In the rotating frame the included energy term can be written as

$$\mathcal{E} = Ze\langle\Phi_0\rangle - \frac{1}{2} m\omega_\varphi^2 \left(R^2 - R_0^2 \right) \ , \tag{3.30}$$

where $\langle \cdot \rangle$ denotes flux-surface averaging, ω_φ the plasma rotation frequency [Eq. (2.13)], R the local major radius and R_0 is an integration constant which can be chosen, i.e. major radius of the Tokamak or flux surface average of the major radius. The Maxwellian is given by the following expression

$$F_0 = F_\mathrm{M}(\mathbf{X}, v_\parallel, \mu) = \frac{n_{R_0}}{(2\pi T/m)^{3/2}} \exp\left(-\frac{\frac{1}{2}m(v_\parallel - u_\parallel)^2 + \mu B_0 + \mathcal{E}}{T} \right) \ , \tag{3.31}$$

where n_{R_0} is the particle density at the position $R = R_0$ and is related to equilibrium particle density through the relation $n_0 = n_{R_0} \exp(-\mathcal{E}/T)$.[19] Furthermore, $u_\parallel$ is the rotation speed of the plasma in the rotating frame parallel to the magnetic field [Eq. (2.14)]. The Maxwellian can seperated in

$$F_\mathrm{M}(\mathbf{X}, v_\parallel, \mu) = F_\mathrm{M}(v_\parallel) F_\mathrm{M}(\mu) e^{-\mathcal{E}/T}, \tag{3.32}$$

$$F_\mathrm{M}(v_\parallel) = \frac{n_{R_0}}{(2\pi T/m)^{3/2}} \exp\left(-\frac{\frac{1}{2}m(v_\parallel - u_\parallel)^2}{T} \right) \qquad F_\mathrm{M}(\mu) = \exp\left(-\frac{\mu B_0}{T} \right) \tag{3.33}$$

and the derivatives of the Maxwellian can be expressed as

$$\begin{aligned}\nabla F_{\mathrm{M}} = &\left[\frac{\nabla n_{R_0}}{n_{R_0}} + \left(\frac{\frac{1}{2}mv_\parallel^2 + \mu B_0 + \mathcal{E}}{T} - \frac{3}{2}\right)\frac{\nabla T}{T} - \frac{\mu B_0}{T}\frac{\nabla B_0}{B_0}\right.\\ &\left. + \left(\frac{mv_\parallel R B_{\mathrm{t}}}{BT} + m\omega\left(R^2 - R_0^2\right)\right)\nabla\omega_\varphi\right] F_{\mathrm{M}}\\ \partial_{v_\parallel} F_{\mathrm{M}} = &-\frac{mv_\parallel}{T}F_{\mathrm{M}}\\ \partial_\mu F_{\mathrm{M}} = &-\frac{B_0}{T}F_{\mathrm{M}}\ ,\end{aligned} \tag{3.34}$$

where the $\nabla\omega_\varphi$-terms are the result of the derivatives of the parallel rotation velocity $u_\parallel$ and rotation energy $\mathcal{E}$ evaluated at zero rotation speed locally in the co-rotating frame.[19] It can be shown with Equations (3.24) and (3.34) that the ∇B_0-term in $-\dot{\mathbf{X}}\cdot\nabla F_{\mathrm{M}}$ cancels with $(\dot{\mathbf{X}}/mv_\parallel)\mu\nabla B_0\partial_{v_\parallel}F_{\mathrm{M}}$ for purely toroidal rotation. Finally, the Vlasov equation (gyrokinetic equation) can than be written as

$$\frac{\partial F_1}{\partial t} + \dot{\mathbf{X}}\cdot\nabla F_1 - \frac{\mathbf{b}_0}{m}\cdot\left(Ze\nabla\Phi_0 + \mu\nabla B_0 - mR\Omega^2\nabla R\right)\cdot\frac{\partial F_1}{\partial v_\parallel} = S$$

$$\begin{aligned}S = &-(\mathbf{v}_\chi + \mathbf{v}_{\mathrm{D}})\cdot\widetilde{\nabla}F_{\mathrm{M}} - \frac{Zev_\parallel}{T}\frac{\partial\bar{A}_{1\parallel}}{\partial t}F_{\mathrm{M}}\\ &-\frac{F_{\mathrm{M}}}{T}(v_\parallel\mathbf{b}_0 + \mathbf{v}_{\mathrm{D}} + \mathbf{v}_{\bar{B}_{1\perp}})\cdot(Ze\nabla\bar{\Phi} + \mu\nabla\bar{B}_{1\parallel})\ ,\end{aligned} \tag{3.35}$$

where $\widetilde{\nabla}$ referes to only the ∇n_{R_0}, ∇T and $\nabla\omega_\varphi$-terms of ∇F_{M}.

3.4 Maxwell's Equations

To obtain a closed system the Vlasov equation gets combined with the Maxwell equations to calculate the perturbated electromagnetic fields. As usual in fusion plasma the Coulomb law gets replaced by the quasi neutrality condition which implies that any deviation from neutrality can only happen on small length scales within the Debye length and on a timescale much shorter than of the fluctuations. Due to the non-relativistic timescale of the turbulence the displacement current in Ampere's law is neglected as well. Taking everything into account the Maxwell's equations can be written as

$$\begin{aligned} \sum_s Z_s e\, n_s = 0 \qquad & \nabla \times \mathbf{E}_1 = -\frac{\partial \mathbf{B}_1}{\partial t} \\ \nabla \cdot \mathbf{B}_1 = 0 \qquad & \nabla \times \mathbf{B}_1 = \mu_0 \sum_s \mathbf{j}_s \ , \end{aligned} \tag{3.36}$$

where the index s refers to the species of particles, i.e. proton or electron and $\sum_s$ means that all species will be taken into account. For simplicity of the derivation the "s" index is dropped if not explicitly needed. The Maxwell's equations contain densities n and currents $\mathbf{j}$ of the particles which can be expressed through the moments of the particle phase space distribution function f as follows

$$n(\mathbf{x}) = \int \mathrm{d}\mathbf{v}\ f(\mathbf{x}, \mathbf{v}) \tag{3.37}$$

$$j_\parallel = Ze \int \mathrm{d}\mathbf{v}\ v_\parallel f(\mathbf{x}, \mathbf{v}) \qquad \mathbf{j}_\perp = Ze \int \mathrm{d}\mathbf{v}\ \mathbf{v}_\perp f(\mathbf{x}, \mathbf{v}) \ . \tag{3.38}$$

3.5 Pull Back Operation into the Guiding Center Phase Space

Since the Vlasov equation [Eq. (3.29)] describes the evolution of the distribution function in the gyrocenter phase space F, the particle moments will be expressed with the guiding center phase space distribution function F^{gc} which will be described through the gyrocenter distribution function F by performing a pull back from F to the guiding center phase space. A schematic about the general idea can be seen in Figure 3.2. The pull back will be performed with the pull back operator $\mathcal{P}$ which results in

$$F^{\mathrm{gc}} = \mathcal{P}\left\{F\right\} = F \underbrace{-\frac{F_{\mathrm{M}}}{T}\left(Ze\widetilde{\Phi}_1 - \mu \bar{B}_{1\parallel}\right)}_{\text{Correction Term}}, \tag{3.39}$$

where $\widetilde{\Phi}_1$ donates to the oscillating part of the perturbation Φ_1. Here, the correction term contains the fluctuations of the electro-magnetic fields and describes physical the polarization and magnetization effects of the fluctuations on the gyro orbit.[2]

Figure 3.2: Schematic to express the Maxwell's equations with gyrocenter distribution F in the guiding center phase space. Here, the particle density $n(\mathbf{x})$, the current density $\mathbf{j}(\mathbf{x})$ and the gyrocenter distribution function F are expressed in the guiding center phase space.

The particle density n and currents $\mathbf{j}$ of one species can be expressed with the guiding center distribution function F^{gc} as

$$\begin{aligned}
n &= \int \mathrm{d}\mathbf{v}\ f(\mathbf{x},\mathbf{v}) = \frac{B_0}{m}\int \mathrm{d}\mathbf{X}\mathrm{d}v_\parallel \mathrm{d}\theta \mathrm{d}\mu\ \delta(\mathbf{X}+\mathbf{r}-\mathbf{x})F^{\mathrm{gc}} \\
j_\parallel &= Ze\int \mathrm{d}\mathbf{v}\ v_\parallel f(\mathbf{x},\mathbf{v}) = \frac{ZeB_0}{m}\int \mathrm{d}\mathbf{X}\mathrm{d}v_\parallel \mathrm{d}\theta \mathrm{d}\mu\ \delta(\mathbf{X}+\mathbf{r}-\mathbf{x})v_\parallel F^{\mathrm{gc}} \\
\mathbf{j}_\perp &= Ze\int \mathrm{d}\mathbf{v}\ \mathbf{v}_\perp f(\mathbf{x},\mathbf{v}) = \frac{ZeB_0}{m}\int \mathrm{d}\mathbf{X}\mathrm{d}v_\parallel \mathrm{d}\theta \mathrm{d}\mu\ \delta(\mathbf{X}+\mathbf{r}-\mathbf{x})\mathbf{v}_\perp F^{\mathrm{gc}}\ ,
\end{aligned} \tag{3.40}$$

where B_0/m is the Jacobian of the guiding center coordinates. The delta function δ appears due to the change of coordinates and ensures that the spatial region taken into account in the integral remains unchanged during the coordinate transformation. Physically, the delta function δ expresses that all particles with a Larmor orbit contribute to the particle density as they crossing a given point $\mathbf{x}$ in the real space [Fig. 3.3].

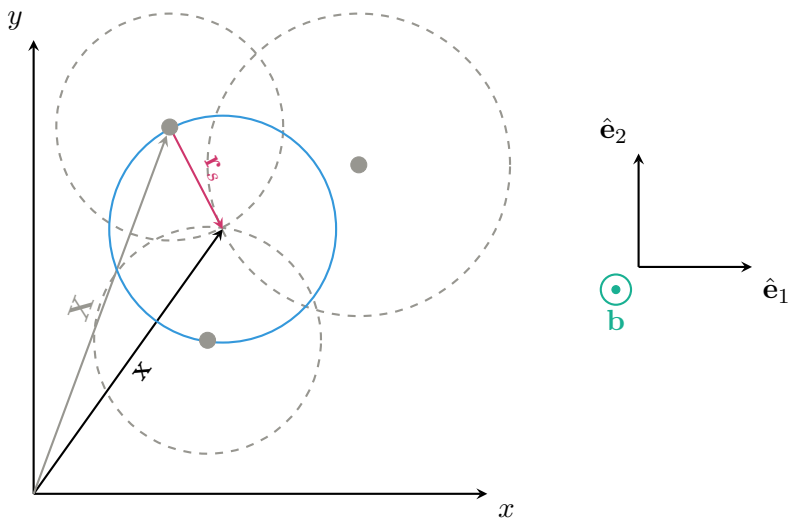

Figure 3.3: Connection between density of particles $n_s(\mathbf{x})$ and density of guiding centers: Gyro orbits with different guiding center $\mathbf{X}$ (gray dashed circles) can cross in postion $\mathbf{x}$, resulting in the respective gyrating particles adding to the particle density n_s of the position $\mathbf{x}$. For a fixed Larmor radius $\rho_s = |\mathbf{r}_s| = |\rho_s \mathbf{a}|$ (red) the particle density n_s at $\mathbf{x}$ is obtained by collecting the contributions of all guiding centers on a circle with radius ρ_s centered at position $\mathbf{x}$ (blue circle).

3.6 Gyrooperator $\mathcal{G}$

As stated in Chapter 3.2.2 the gyrooperator $\mathcal{G}$ averages over the gyrophase θ which is mostly used in the derivation of the field equation and is defined as

$$\mathcal{G}\{G(\mathbf{x})\} = \bar{G}(\mathbf{X}) = \frac{1}{2\pi}\int_0^{2\pi} \mathrm{d}\theta \; G(\mathbf{X} + \mathbf{r}(\theta)) \; . \tag{3.41}$$

To derive the field equations, a second kind of gyrooperator will be introduced as

$$\mathcal{G}^\dagger\{G(\mathbf{X})\} = \langle G \rangle(\mathbf{x}) = \frac{1}{2\pi}\int_0^{2\pi} \mathrm{d}\mathbf{X}\mathrm{d}\theta \; \delta(\mathbf{X} + \mathbf{r}(\theta) - \mathbf{x}) G(\mathbf{X}) \; , \tag{3.42}$$

where $\mathcal{G}^\dagger$ the hermitian conjugate of $\mathcal{G}$[24] and the delta function δ originates from the pull back operation from Chapter 3.5.[14] Furthermore, the double gyroaverage operator is defined as

$$\mathcal{G}^\dagger\big\{\mathcal{G}\{G(\mathbf{x})\}\big\} = \langle \bar{G} \rangle(\mathbf{x}) = \frac{1}{(2\pi)^2}\int_0^{2\pi} \mathrm{d}\theta \int_0^{2\pi} \mathrm{d}\theta' \; G(\mathbf{X} - \mathbf{r}(\theta) + \mathbf{r}(\theta')) \; , \tag{3.43}$$

which performs a gyroaverage of the field value at all guiding center positions $\mathbf{X}$ with particle position $\mathbf{x}$ in their trajectory.[13]

In the case of local simulations the gyrooperators $\mathcal{G}$ and $\mathcal{G}^\dagger$ is simplified to

$$\begin{aligned} \bar{\mathbf{G}}(\mathbf{x}) &= J_0(\lambda)\mathbf{G}(\mathbf{X}) \\ \langle \mathbf{G}(\mathbf{X}) \rangle &= J_0(\lambda)\mathbf{G}(\mathbf{x}) \end{aligned} \tag{3.44}$$

with J_0 as the zeroth order Bessel function. Note, that $\bar{B}_{1\parallel}(\mathbf{X}) = -I_1(\lambda)\mu B_{1\parallel}(\mathbf{X})$, where I_1 is the modified first order Bessel function of first kind defined as $I_1(\lambda) = 2/\lambda \, J_1(\lambda)$. To obtain Equation (3.44) the process of gyroaveraging will be performend in the Fourier space as follows

$$\begin{aligned} \bar{\mathbf{G}}(\mathbf{x}) = \bar{\mathbf{G}}(\mathbf{X} + \mathbf{r}) &= \mathcal{G}\left\{ \int \mathrm{d}\mathbf{k} \; \hat{\mathbf{G}}(\mathbf{k}) e^{i\mathbf{k}\cdot(\mathbf{X}+\mathbf{r})} \right\} \\ &= \frac{1}{2\pi}\int_0^{2\pi} \mathrm{d}\theta \; \int \mathrm{d}\mathbf{k} \; \hat{\mathbf{G}}(\mathbf{k}) e^{i\mathbf{k}\cdot\mathbf{X}} e^{ik_\perp \rho \cos\theta} \\ &= \int \mathrm{d}\mathbf{k} \; \hat{\mathbf{G}}(\mathbf{k}) e^{i\mathbf{k}\cdot\mathbf{X}} \underbrace{\frac{1}{2\pi}\int_0^{2\pi} \mathrm{d}\theta \; e^{ik_\perp \rho \cos\theta}}_{J_0(\rho k_\perp)} \\ &= \int \mathrm{d}\mathbf{k} \; J_0(\rho k_\perp) \hat{\mathbf{G}}(\mathbf{k}) e^{i\mathbf{k}\cdot\mathbf{X}} = J_0(\lambda)\mathbf{G}(\mathbf{X}) \; , \end{aligned} \tag{3.45}$$

with the wave vector $\mathbf{k}$ defined as $\mathbf{k} = \hat{e}_1 k_\perp$. The argument λ is given by $i\rho\nabla_\perp$ as the inverse Fourier transformated expression of $\rho k_\perp$. The same routine can be applied for the gyrooperator $\mathcal{G}^\dagger$ with the same result. In general the Bessel function is defined as[6]

$$\begin{aligned} J_n(z) &= \left(\frac{z}{2}\right)^n \underbrace{\sum_{\nu=0}^{\infty} \frac{\left(\left(-1/4z^2\right)^\nu\right)}{\nu!(1+\nu)!}}_{I_n(z)} , \\ J_n(z) &= \frac{i^{-n}}{\pi} \int_0^\pi \mathrm{d}\theta \; e^{iz\cos\theta} \cos(n\theta) \; . \end{aligned} \tag{3.46}$$

Integrals with Bessel Function

In the upcoming section there will be multiple integrals containing the zeroth-order Bessel function $J_0(\lambda)$ and the modified Bessel functions $I_1(\lambda)$. In general these types of integrals have the form

$$\int \mathrm{d}v_\parallel \mathrm{d}\mu \; v_\parallel^m \mu^n J_0^{2-n}(\lambda) I_1^n(\lambda) F_\mathrm{M}, \tag{3.47}$$

with the natural number $n,\ m = \{0, 1, 2\}$. Equation (3.47) can be seperated by using the Maxwellian [Eq. (3.33)] to form

$$e^{-\mathcal{E}/T} \int \mathrm{d}v_\parallel \; v_\parallel^m F_\mathrm{M}(v_\parallel) \int \mathrm{d}\mu \; \mu^n J_0^{2-n}(\lambda) I_1^n(\lambda) F_\mathrm{M}(\mu) \; . \tag{3.48}$$

The first integral appears in the following types

$$\begin{aligned} &1) \int \mathrm{d}v_\parallel \; F_\mathrm{M}(v_\parallel) && = \frac{n_{R_0} m}{2\pi T} \\ &2) \int \mathrm{d}v_\parallel \; v_\parallel F_\mathrm{M}(v_\parallel) && = 0 \qquad \text{(Due to symmetry)} \\ &3) \int \mathrm{d}v_\parallel \; v_\parallel^2 F_\mathrm{M}(v_\parallel) && = \frac{n_{R_0}}{2\pi} \end{aligned} \tag{3.49}$$

and the last integral occurs in three types

$$\begin{aligned} &1) \int \mathrm{d}\mu \; J_0^2(\lambda) F_\mathrm{M}(\mu) && = \frac{T}{B_0} \Gamma_0(b) \\ &2) \int \mathrm{d}\mu \; \mu J_0(\lambda) I_1(\lambda) F_\mathrm{M}(\mu) && = \frac{T^2}{B_0^2} (\Gamma_0(b) - \Gamma_1(b)) \\ &3) \int \mathrm{d}\mu \; \mu^2 I_1^2(\lambda) F_\mathrm{M}(\mu) && = \frac{T^3}{B_0^3} 2(\Gamma_0(b) - \Gamma_1(b)) \; , \end{aligned} \tag{3.50}$$

with the notation $\Gamma_n(b) = I_n(b) e^{-b}$ with the modified Bessel function I_n [Eq. (3.46)] and $b = -\rho_\mathrm{th}^2 \nabla^2{}_\perp$. ρ_th referes to the thermal Larmor radius [Eq. (2.4)].[23]

3.7 Normalization

To implement the field equations into the local version of GKW, one has to normalize the quantities in the equations. The reference values are indicated by the index "ref", the dimensionless normalized by "N" and the relative dimensionless values by the index "R". This section is based on Ref 4, 23 and 17.

A reference mass m_{ref}, density n_{ref}, temperature T_{ref}, magnetic field B_{ref} and major radius R_{ref} are chosen. With these quantities the reference thermal velocity $v_{\mathrm{th,ref}}$ and reference thermal Larmor radius $\rho_{\mathrm{th,ref}}$ are defined as

$$T_{\mathrm{ref}} = \frac{1}{2} m_{\mathrm{ref}} v_{\mathrm{th,ref}}^2 \qquad \rho_{\mathrm{th,ref}} = \frac{m_{\mathrm{ref}} v_{\mathrm{th,ref}}}{e B_{\mathrm{ref}}} = \frac{2 T_{\mathrm{ref}}}{e B_{\mathrm{ref}} v_{\mathrm{th,ref}}} \qquad \rho_\star = \frac{\rho_{\mathrm{th,ref}}}{R_{\mathrm{ref}}}$$

and for convenience the small parameter $\rho_\star$ are redefined.

- **Relative Quantities:**

$$m = m_{\mathrm{ref}} m_{\mathrm{R}} \qquad n_{R_0} = n_{\mathrm{ref}} n_{\mathrm{R}} \qquad T = T_{\mathrm{ref}} T_{\mathrm{R}} \qquad v_{\mathrm{th}} = v_{\mathrm{th,ref}} v_{\mathrm{thR}}$$

- **Normalized Quantities:**

$$R = R_{\mathrm{ref}} R_{\mathrm{N}} \qquad B_0 = B_{\mathrm{ref}} B_{\mathrm{N}} \qquad \mu = \frac{2 T_{\mathrm{ref}} T_{\mathrm{R}}}{B_{\mathrm{ref}}} \mu_{\mathrm{N}} \qquad v_\parallel = v_{\mathrm{th}} v_{\parallel \mathrm{N}}$$

$$k = \frac{k_{\mathrm{N}}}{\rho_\star} \qquad k_\parallel = \frac{k_{\parallel \mathrm{N}}}{\rho_\star} \qquad k_\perp = \frac{k_{\perp \mathrm{N}}}{\rho_{\mathrm{th,ref}}}$$

$$\beta = \beta_{\mathrm{ref}} \beta_{\mathrm{N}} \qquad \beta_{\mathrm{ref}} = \frac{2 \mu_0 n_{\mathrm{ref}} T_{\mathrm{ref}}}{B_{\mathrm{ref}}^2}$$

  - **Fluctuating Fields:**

$$\Phi_1 = \rho_\star \frac{T_{\mathrm{ref}}}{e} \Phi_{1\mathrm{N}} \qquad B_{1\parallel} = \rho_\star B_{\mathrm{ref}} B_{1\parallel \mathrm{N}}$$

$$A_{1\parallel} = B_{\mathrm{ref}} R_{\mathrm{ref}} \rho_\star^2 A_{1\parallel \mathrm{N}} \qquad E_{1\parallel} = \frac{2 T_{\mathrm{ref}}}{e} \frac{1}{R_{\mathrm{ref}}} \rho_\star E_{1\parallel \mathrm{N}}$$

  - **Time, Frequency and Centrifugal Energy:**

$$t = \frac{R_{\mathrm{ref}}}{v_{\mathrm{th,ref}}} t_{\mathrm{N}} \qquad \Omega = \frac{v_{\mathrm{th,ref}}}{R_{\mathrm{ref}}} \Omega_{\mathrm{N}} \qquad \mathcal{E} = T_{\mathrm{ref}} \mathcal{E}_{\mathrm{N}}$$

  - **Distribution Function and Vlasov Equation:**

$$F = \rho_\star \frac{n_{R_0}}{v_{\mathrm{th}}^3} F_{\mathrm{N}} \qquad F_{\mathrm{M}} = \frac{n_{R_0}}{v_{\mathrm{th}}^3} F_{\mathrm{MN}} \qquad \mathcal{V} = \rho_\star \frac{v_{\mathrm{th,ref}}}{R_{\mathrm{ref}}} \frac{n_{R_0}}{v_{\mathrm{th}}^3} \mathcal{V}_{\mathrm{N}}$$

  - **Gradients:**

$$\nabla_\perp = \frac{1}{R_{\mathrm{ref}}} \nabla_{\perp \mathrm{N}} \qquad \nabla_\parallel = \frac{1}{R_{\mathrm{ref}}} \nabla_{\parallel \mathrm{N}} \ .$$

3.8 Field Equations

3.8.1 Coulomb's Law - Perturbated Electrostatic Potential Φ_1

To evaluate the perturbated electrostatic potential Φ_1 in the gyrocenter phase space Equation (3.39) is inserted into the equation for the particle density $n(\mathbf{x})$, which results in

$$\begin{aligned} n_1(\mathbf{x}) &= \frac{B_0}{m}\int \mathrm{d}\mathbf{X}\mathrm{d}v_\parallel \mathrm{d}\theta \mathrm{d}\mu\ \delta(\mathbf{X}+\mathbf{r}-\mathbf{x})\left(F_1 - \frac{F_\mathrm{M}}{T}\left(Ze\widetilde{\Phi}_1 - \mu\bar{B}_{1\parallel}\right)\right) \\ &= \bar{n}_1(\mathbf{x}) + n_\mathcal{P}(\mathbf{x})\ , \end{aligned} \tag{3.51}$$

with the density of the gyrocenter $\bar{n}_1(\mathbf{x})$ and the variations on the gyro orbit related to the particle density $n_\mathcal{P}(\mathbf{x})$, which describes the polarization effects of the fluctuating fields on the gyro orbit[2]. The gyrocenter density can be simplyfied with the gyroperator $\mathcal{G}^\dagger$ [Eq. (3.42)] to

$$\bar{n}_1(\mathbf{x}) = \frac{B_0}{m}\int \mathrm{d}\mathbf{X}\mathrm{d}v_\parallel\mathrm{d}\theta\mathrm{d}\mu\ \delta(\mathbf{X}+\mathbf{r}-\mathbf{x})F_1 = \frac{2\pi B_0}{m}\int \mathrm{d}v_\parallel\mathrm{d}\mu\ \langle F_1\rangle\ . \tag{3.52}$$

The polarization density $n_\mathcal{P}$ is given by

$$n_\mathcal{P}(\mathbf{x}) = -\frac{2\pi B_0}{m}\int \mathrm{d}v_\parallel\mathrm{d}\mu\ \frac{F_\mathrm{M}}{T}\left(Ze\left(\Phi_1(\mathbf{x}) - \langle\bar{\Phi}_1\rangle(\mathbf{x})\right) - \mu\langle\bar{B}_{1\parallel}\rangle\right)\ . \tag{3.53}$$

To derive the term for the polarization density $n_\mathcal{P}$, the oscillating part of the electrostatic potential is replaced with $\widetilde{\Phi}_1(\mathbf{X}+\mathbf{r}) = \Phi_1(\mathbf{X}+\mathbf{r}) - \bar{\Phi}_1(\mathbf{X})$ and the gyrooperator $\mathcal{G}^\dagger$ is applied. Taking everything into account and inserting it into the quasi neutrality equation $\sum_s Z_s e\, n_{1,s} = 0$ the field equation for the perturbated electrostatic potential Φ_1 is given by

$$\begin{aligned} &\sum_s \frac{Z_s^2 e^2}{m_s}\int \mathrm{d}v_\parallel\mathrm{d}\mu\ \frac{F_{\mathrm{M},s}}{T_s}\left(\Phi_1(\mathbf{x}) - \langle\bar{\Phi}_1\rangle(\mathbf{x})\right) = \\ &\sum_s \frac{Z_s e}{m_s}\int \mathrm{d}v_\parallel\mathrm{d}\mu\ \langle F_{1,s}\rangle + \frac{F_{\mathrm{M},s}}{T_s}\mu\langle\bar{B}_{1\parallel}\rangle\ . \end{aligned} \tag{3.54}$$

With the use of the local gyrooperator $\mathcal{G}$ the density of the gyrocenter $\bar{n}_1$ and the polarization density $n_\mathcal{P}$ can be expressed as

$$\bar{n}_1(\mathbf{x}) = \frac{2\pi B_0}{m}\int \mathrm{d}v_\parallel\mathrm{d}\mu\ J_0(\lambda)F_1(\mathbf{x}, v_\parallel, \mu)\ , \tag{3.55}$$

$$\begin{aligned} n_\mathcal{P}(\mathbf{x}) =& \frac{Zen_{R_0}(\mathbf{x})}{T}e^{-\mathcal{E}/T}(\Gamma_0(b)-1)\Phi_1(\mathbf{x}) \\ &+ n_{R_0}(\mathbf{x})e^{-\mathcal{E}/T}(\Gamma_0(b)-\Gamma_1(b))\frac{B_{1\parallel}(\mathbf{x})}{B_0}\ , \end{aligned} \tag{3.56}$$

where n_{R_0} is the background density at postion R_0. To derive the term for the polarization density $n_{\mathcal{P}}$ the integrals mentioned in Chapter 3.6 are applied. Then, the field equation for the perturbated electrostatic potential Φ_1 in the local simulation is given by

$$\begin{aligned}&\sum_s \frac{Z_s^2 e^2}{T_s} n_{R_0,s} e^{-\mathcal{E}_s/T_s} \left(1-\Gamma_0(b_s)\right) \Phi_1(\mathbf{x}) = \\ &\sum_s Z_s e \left(\bar{n}_{1,s} + n_{R_0,s} e^{-\mathcal{E}_s/T_s} (\Gamma_0(b_s) - \Gamma_1(b_s)) \frac{B_{1\parallel}(\mathbf{x})}{B_0} \right)\end{aligned} \tag{3.57}$$

and takes the following form after performing the Fourier-transform and applying the normalizing expressions [Ch. 3.7]

$$\begin{aligned}&\sum_s Z_s n_{\mathrm{R},s} e^{-\mathcal{E}_{\mathrm{N},s}/T_{\mathrm{R},s}} \left(1-\Gamma_0(b_s)\right) \frac{Z_s}{T_{\mathrm{R},s}} \widehat{\Phi}_{1\mathrm{N}} = \\ &\sum_s Z_s n_{\mathrm{R},s} 2\pi B_{\mathrm{N}} \int \mathrm{d}v_{\parallel \mathrm{N}} \mathrm{d}\mu_{\mathrm{N}} \; J_0(k_\perp \rho_s) \widehat{F}_{1\mathrm{N},s} \\ &+ \sum_s Z_s n_{\mathrm{R},s} e^{-\mathcal{E}_{\mathrm{N},s}/T_{\mathrm{R},s}} (\Gamma_0(b_s) - \Gamma_1(b_s)) \frac{\widehat{B}_{1\parallel \mathrm{N}}}{B_{\mathrm{N}}}\end{aligned} \tag{3.58}$$

3.8.2 Perpendicular Ampere's Law - Magnetic Compression $B_{1\parallel}$

The perpendicular compentent of Ampere's law can be written as

$$\nabla^2 \mathbf{A}_{1\perp} = (\nabla \times B_{1\parallel})_\perp = \begin{pmatrix} \partial_y B_{1\parallel} - \partial_z B_{1y} \\ \partial_z B_{1x} - \partial_x B_{1\parallel} \end{pmatrix} = -\mu_0 \mathbf{j}_{1\perp} \ , \tag{3.59}$$

where z is the direction of the equilibrium magnetic field B_0 and the Coulomb gauge $\nabla \cdot \mathbf{A}_1 = 0$ is used. The parallel gradients of the perturbated magnetic field can be neglected since they are one order smaller than the perpendicular ones, which results in

$$\begin{pmatrix} \partial_y B_{1\parallel} \\ -\partial_x B_{1\parallel} \end{pmatrix} = \nabla_\perp B_{1\parallel} \times \mathbf{b} = -\mu_0 \mathbf{j}_{1\perp} \ . \tag{3.60}$$

After performing the pull back operation the perpendicular current $\mathbf{j}_{1\perp}$ is given by

$$\mathbf{j}_{1\perp} = \frac{ZeB_0}{m} \int \mathrm{d}\mathbf{X} \mathrm{d}v_\parallel \mathrm{d}\theta \mathrm{d}\mu \ \delta(\mathbf{X} + \mathbf{r} - \mathbf{x}) \mathbf{v}_\perp \left(F_1 - \frac{F_\mathrm{M}}{T} \left(Ze\widetilde{\Phi}_1 - \mu \bar{B}_{1\parallel} \right) \right) \ . \tag{3.61}$$

Inserting the perturbated perpenedicular current $\mathbf{j}_{1\perp}$ into Ampere's law and applying the same method as in Ref. 23 results in the field equation for the perturbated parallel magnetic field $B_{1\parallel}$, which can be expressed as

$$\begin{aligned} &\left(1 + \sum_s \beta_s (\Gamma_0(b_s) - \Gamma_1(b_s)) e^{-\mathcal{E}_s/T_s} \right) B_{1\parallel} = \\ &- \sum_s \frac{2\pi\mu_0 B_0}{m_s} \int \mathrm{d}v_\parallel \mathrm{d}\mu \ \mu I_n(\lambda_s) F_{1,s} \\ &- \sum_s (\Gamma_0(b_s) - \Gamma_1(b_s)) e^{-\mathcal{E}_s/T_s} \frac{Z_s e \mu_0 n_{R_0,s}}{B_0} \Phi_1 \ , \end{aligned} \tag{3.62}$$

with β_s as the plasma beta of a given species. Using Fourier transformation and normalization yield

$$\begin{aligned} &\left(1 + \sum_s \frac{T_{\mathrm{R},s} n_{\mathrm{N},s}}{B_\mathrm{N}^2} \beta_\mathrm{ref} (\Gamma_0(b_s) - \Gamma_1(b_s)) e^{-\mathcal{E}_{\mathrm{N},s}/T_{\mathrm{R},s}} \right) \widehat{B}_{1\parallel\mathrm{N}} = \\ &- \sum_s \beta_\mathrm{ref} 2\pi B_\mathrm{N} T_{\mathrm{R},s} n_{\mathrm{R},s} \int \mathrm{d}v_{\parallel\mathrm{N}} \mathrm{d}\mu_\mathrm{N} \ \mu_\mathrm{N} I_1(k_\perp \rho_s) \widehat{F}_{1\mathrm{N},s} \\ &- \sum_s \beta_\mathrm{ref} (\Gamma_0(b_s) - \Gamma_1(b_s)) e^{-\mathcal{E}_{\mathrm{N},s}/T_{\mathrm{R},s}} \frac{Z_s n_{\mathrm{R},s}}{2B_\mathrm{N}} \widehat{\Phi}_{1\mathrm{N}} \ . \end{aligned} \tag{3.63}$$

3.8.3 Parallel Ampere's Law - Vector Potential $A_{1\parallel}$

To express the parallel perturbation of the vector potential $A_{1\parallel}$, the method is analogous to Chapter 3.8.1. The parallel compentent of Ampere's law can be expressed as

$$\nabla^2 A_{1\parallel} = -\mu_0 j_{1\parallel} = -\mu_0 \sum_s j_{1\parallel,s} \ . \tag{3.64}$$

Performing the pull back again the parallel perturbation of the current density $j_{1\parallel}$ is given by

$$\begin{aligned} j_{1\parallel} &= \frac{ZeB_0}{m} \int \mathrm{d}\mathbf{X}\mathrm{d}v_\parallel \mathrm{d}\theta \mathrm{d}\mu \ \delta(\mathbf{X}+\mathbf{r}-\mathbf{x}) v_\parallel \left(F_1 - \frac{F_\mathrm{M}}{T} \left(Ze\widetilde{\Phi}_1 - \mu \bar{B}_{1\parallel} \right) \right) \\ &= \frac{ZeB_0}{m} \int \mathrm{d}\mathbf{X}\mathrm{d}v_\parallel \mathrm{d}\theta \mathrm{d}\mu \ \delta(\mathbf{X}+\mathbf{r}-\mathbf{x}) v_\parallel F_1 \\ &= \frac{2\pi ZeB_0}{m} \int \mathrm{d}v_\parallel \mathrm{d}\mu \ \langle v_\parallel F_1 \rangle \ , \end{aligned} \tag{3.65}$$

although the term $v_\parallel F_\mathrm{M}$ vanishes during the integration along $v_\parallel$, due to symmetry of the Maxwellian F_M. Inserting Equation (3.65) into Ampere's law yields the field equation for the perturbated vector potential $A_{1\parallel}$ as follows

$$\nabla^2 A_{1\parallel} = -\sum_s \frac{2\pi Z_s e \mu_0 B_0}{m_s} \int \mathrm{d}v_\parallel \mathrm{d}\mu \ \langle v_\parallel F_{1,s} \rangle \tag{3.66}$$

and after the use of the local gyroperator definition

$$\nabla^2 A_{1\parallel} = -\sum_s \frac{2\pi Z_s e \mu_0 B_0}{m_s} \int \mathrm{d}v_\parallel \mathrm{d}\mu \ v_\parallel J_0(\lambda_s) F_{1,s}(\mathbf{x}, v_\parallel, \mu) \ . \tag{3.67}$$

The Fourier transformation and normalization yield

$$k_{\perp\mathrm{N}}^2 \widehat{A}_{1\parallel\mathrm{N}} = 2\pi B_\mathrm{N} \beta_\mathrm{ref} \sum_s Z_s n_{\mathrm{R},s} v_{\mathrm{thR},s} \int \mathrm{d}v_{\parallel\mathrm{N}} \mathrm{d}\mu_\mathrm{N} \ v_{\parallel\mathrm{N}} J_0(k_\perp \rho_s) \widehat{F}_{1\mathrm{N},s} \ . \tag{3.68}$$

3.8.4 Cancellation Problem

Local and global Gyrokinetic simulations are suffering from numerical problems, mainly from saturation of the heat fluxes at a high level of transport (nonzonal transition (NZT)) and the cancellation problem[3]. The cancellation problem is examined in codes which uses the particle-in-cell or the Eulerian methods[5]. In the following chapter the origin of the cancellation problem will be discussed.

As discussed in Chapter 3.3.2 the time derivative of the parallel pertrubed vector potential $\partial_t \bar{A}_{1\parallel}$ appears in the Source term [Eq. (3.35)]. This $\partial t A_{1\parallel}$-term and the $\partial t F_1$-term in the gyrokinetic equation are computationally difficult to handle, as it is not immediately clear how to evaluate the terms by using a simple Runge-Kutta scheme. To avoid further complications a modified distribution function g is introduced

$$g = F_1 + \frac{Zev_\parallel}{T}\bar{A}_{1\parallel}F_\mathrm{M} \ . \tag{3.69}$$

Substituting the modified distribution function g into Equation (3.29) results in

$$\frac{\partial g}{\partial t} + \mathbf{v}_\chi \cdot \nabla g + (v_\parallel \mathbf{b}_0 + \mathbf{v}_\mathrm{D}) \cdot \nabla F_1 - \frac{\mathbf{b}_0}{m} \cdot (Ze\nabla\Phi_0 + \mu\nabla B_0 - mR\Omega^2\nabla R)\frac{\partial F_1}{\partial v_\parallel} = S \tag{3.70}$$

with the source term S defined as

$$S = -(\mathbf{v}_\chi + \mathbf{v}_\mathrm{D}) \cdot \tilde{\nabla} F_\mathrm{M} - \frac{F_\mathrm{M}}{T}(v_\parallel \mathbf{b}_0 + \mathbf{v}_\mathrm{D}) \cdot (Ze\nabla\bar{\Phi} + \mu\nabla\bar{B}_{1\parallel}) \ . \tag{3.71}$$

The advantage of this substitution becomes apperent as now only one time derivative appears in the gyrokinetic equation. Due to the substitution the distribution function F_1 in the field equations has to be replaced with the modified distribution g as

$$F_1 = g - \frac{Zev_\parallel}{T}\bar{A}_{1\parallel}F_\mathrm{M} \ . \tag{3.72}$$

For the equations of perturbated electrostatic potential Φ_1 and parallel magnetic field $B_{1\parallel}$ the replacement is trivial since the integral $\int \mathrm{d}v_\parallel v_\parallel F_\mathrm{M} = 0$ (due to symmetry) results in the elimination of the $A_{1\parallel}$-term in both equation leaving the modified distribution g in the integral. For the field equation for $A_{1\parallel}$ the substitution has a different effect. By replacing F_1 with g the new normalized Fourier transformed field equation for $A_{1\parallel}$ is given by

$$\begin{aligned} &\left(k_{\perp\mathrm{N}}^2 + \beta_\mathrm{ref}\sum_s \frac{Z_s^2 n_{\mathrm{R},s}}{m_{\mathrm{R},s}}\Gamma_0(b_s)e^{-\mathcal{E}_{\mathrm{N},s}/T_{\mathrm{R},s}}\right)\widehat{A}_{1\parallel\mathrm{N}} = \\ &2\pi B_\mathrm{N}\beta_\mathrm{ref}\sum_s Z_s n_{\mathrm{R},s} v_{\mathrm{thR},s}\int \mathrm{d}v_{\parallel\mathrm{N}}\mathrm{d}\mu_\mathrm{N}\ v_{\parallel\mathrm{N}}J_0(k_\perp\rho_s)\widehat{g}_{\mathrm{N},s} \ . \end{aligned} \tag{3.73}$$

Comparing Eq. (3.68) and Eq. (3.73), an additional term in the brackets of Eq. (3.73), the so-called *skin term*[15], appears. It has no physical meaning and only appears due to the substitution of the distribution function. To understand the cancellation problem completely, one has to consider the "hidden" $A_{1\parallel}$-term in the distribution g. This $A_{1\parallel}$-term has to be cancelled exactly with the skin term. But due to the different numerical representation of the skin term (analytically) and the integral over the modified distribution function (numerically), the cancellation is inexact and leads to the cancellation problem. The error of the cancellation scales with $\beta_{\mathrm{ref}}/k_{\perp\mathrm{N}}^2$, making simulations with high plasma beta und small $k_\perp$ very challenging.[16] To mitigate the cancellation problem the gamma function $\Gamma(b)$ is calculated with the same numerical scheme as the integral over the distribution. This approuch has to be performed carefully and may still lead to errors.

3.8.5 Faraday's Law - Plasma Induction $\boldsymbol{E_{1\parallel}}$

In this Chapter the $\partial_t \bar{A}_{1\parallel}$-term will be handled differently with an additional electromagnetic field in mind. This section follows the work of Paul Crandall in chapter 5 of his Disseration[4].

First the Vlasov equation is written for the gyrocenter distribution F_1 with the source term [Eq. (3.29) & (3.35)] and is simplified into

$$\frac{\partial F_1}{\partial t} + \frac{Zev_\parallel}{T}\frac{\partial \bar{A}_{1\parallel}}{\partial t}F_\mathrm{M} = \mathcal{V} \ , \tag{3.74}$$

where $\mathcal{V}$ represents all terms of the Vlasov Equation, which excludes the time derivative of the vector potential $\partial_t \bar{A}_{1\parallel}$ and is called right-hand side (RHS). The equation of the $\bar{A}_{1\parallel}$ is already established in Chapter 3.8.3 but for this derivation a recall will be made. The equation for $\bar{A}_{1\parallel}$ is given by

$$\nabla^2 A_{1\parallel} = -\mu_0 j_{1\parallel} = -\sum_s \frac{2\pi Z_s e \mu_0 B_0}{m_s}\int \mathrm{d}v_\parallel \mathrm{d}\mu \ \langle v_\parallel F_{1,s}\rangle \ . \tag{3.75}$$

Now the Faraday law will be considered

$$E_{1\parallel} = -\frac{\partial A_{1\parallel}}{\partial t} \ . \tag{3.76}$$

Taking the time derivative of Equation (3.75) results directly into the Faraday's law and thereby into the field equation for the plasma induction $E_{1\parallel}$, which can be expressed as

$$\nabla^2 E_{1\parallel} - \sum_s \frac{2\pi Z_s e \mu_0 B_0}{m_s}\int \mathrm{d}v_\parallel \mathrm{d}\mu \ \langle v_\parallel \frac{\partial F_{1,s}}{\partial t}\rangle = 0 \ . \tag{3.77}$$

In Equation (3.77) the time derivative of the gyrocenter distribution function has to be further simplified. For that, the gyrokinetic equation is rewritten as

$$\frac{\partial F_1}{\partial t} = \mathcal{V} + \frac{Zev_\parallel}{T}\bar{E}_{1\parallel}F_\mathrm{M} \ . \tag{3.78}$$

Plugging Equation (3.78) into Equation (3.77), the equation for the plasma induction emerges as

$$\begin{aligned} &\left(\nabla^2 - \sum_s \frac{2\pi (Z_s e)^2 \mu_0 B_0}{T_s m_s}\int \mathrm{d}v_\parallel \mathrm{d}\mu \ \mathcal{G}^\dagger v_\parallel^2 F_{\mathrm{M}s}\mathcal{G}\right) E_{1\parallel} = \\ &\sum_s \frac{2\pi Z_s e \mu_0 B_0}{m_s}\int \mathrm{d}v_\parallel \mathrm{d}\mu \ \mathcal{G}^\dagger \left\{v_\parallel \mathcal{V}_s\right\} = \mu_0 \frac{\partial j_{1\parallel}}{\partial t} \ , \end{aligned} \tag{3.79}$$

although the relation of $\bar{E}_{1\parallel} = \mathcal{G}\left\{E_{1\parallel}\right\}$ and the definition of $\mathcal{G}^\dagger$ was used to simply the integral on the right-hand side. To complete the derivation of this section the delta-*f* Vlasov equation will be recalled with the plasma induction $E_{1\parallel}$ in the source term. The delta-*f* Vlasov equation is given by

$$\frac{\partial F_1}{\partial t} + \dot{\mathbf{X}} \cdot \nabla F_1 - \frac{\mathbf{b}_0}{m} \cdot \left(Ze\nabla\Phi_0 + \mu\nabla B_0 - mR\Omega^2\nabla R\right) \cdot \frac{\partial F_1}{\partial v_\parallel} = S \ , \tag{3.80}$$

with the source term

$$\begin{aligned} S = &-(\mathbf{v}_\chi + \mathbf{v}_\mathrm{D}) \cdot \tilde{\nabla} F_\mathrm{M} + \frac{Zev_\parallel}{T}\bar{E}_{1\parallel}F_\mathrm{M} \\ &-\frac{F_\mathrm{M}}{T}(v_\parallel \mathbf{b}_0 + \mathbf{v}_\mathrm{D} + \mathbf{v}_{\bar{B}_{1\perp}}) \cdot (Ze\nabla\bar{\Phi} + \mu\nabla\bar{B}_{1\parallel}) \ . \end{aligned} \tag{3.81}$$

Using the local definition of the gyrooperator into Equation (3.77), one can derive the equation for the included electric field

$$\begin{aligned} &\left(\nabla^2 - \sum_s \frac{2\pi(Z_s e)^2\mu_0 B_0}{T_s m_s}\int \mathrm{d}v_\parallel \mathrm{d}\mu \ v_\parallel^2 J_0^2(\lambda_s) F_{\mathrm{M}s}\right) E_{1\parallel} = \\ &\sum_s \frac{2\pi Z_s e\mu_0 B_0}{m_s}\int \mathrm{d}v_\parallel \mathrm{d}\mu \ v_\parallel J_0(\lambda_s)\mathcal{V}_s = \mu_0 \frac{\partial j_{1\parallel}}{\partial t} \ . \end{aligned} \tag{3.82}$$

The integral itself can be more simplified with performing the integral over $v_\parallel$ and μ

$$\begin{aligned} I &= \frac{2\pi(Ze)^2\mu_0 B_0}{Tm}\int \mathrm{d}v_\parallel \mathrm{d}\mu \ v_\parallel^2 J_0^2(\lambda) F_\mathrm{M} \\ &= \frac{2\pi(Ze)^2\mu_0 B_0}{Tm} e^{-\mathcal{E}/T} \underbrace{\int \mathrm{d}v_\parallel \ v_\parallel^2 F_\mathrm{M}(v_\parallel)}_{n_{R_0}/2\pi} \underbrace{\int \mathrm{d}\mu \ J_0^2(\lambda) F_\mathrm{M}(\mu)}_{T/B_0 \ \Gamma_0(b)} \\ &= \frac{(Ze)^2\mu_0 n_{R_0}}{m}\Gamma_0(b) e^{-\mathcal{E}/T} \ , \end{aligned} \tag{3.83}$$

where the seperation of the Maxwellian was used [Eq. (3.33)]. Finally, the field equation for the plasma induction can be written as

$$\begin{aligned} &\left(\nabla^2 - \sum_s \frac{Z_s^2 e^2\mu_0 n_{R_0,s}}{m_s}\Gamma_0(b_s) e^{-\mathcal{E}_s/T_s}\right) E_{1\parallel} = \\ &\sum_s \frac{2\pi Z_s e\mu_0 B_0}{m_s}\int \mathrm{d}v_\parallel \mathrm{d}\mu \ v_\parallel J_0(\lambda_s)\mathcal{V}_s = \mu_0 \frac{\partial j_{1\parallel}}{\partial t} \ . \end{aligned} \tag{3.84}$$

After performing the Fouriertransformation and normalization Equation (3.84) the final

field equation for the plasma induction is given by

$$\begin{aligned}\left(k_{\perp\mathrm{N}}^2+\beta_{\mathrm{ref}}\sum_s\frac{Z_s^2 n_{\mathrm{R},s}}{m_{\mathrm{R},s}}\Gamma_0(b_s)e^{-\mathcal{E}_{\mathrm{N},s}/T_{\mathrm{R},s}}\right)\widehat{E}_{1\parallel\mathrm{N}}=\\ -2\pi B_{\mathrm{N}}\beta_{\mathrm{ref}}\sum_s Z_s n_{\mathrm{R},s}v_{\mathrm{thR},s}\int \mathrm{d}v_{\parallel\mathrm{N}}\mathrm{d}\mu_{\mathrm{N}}\; v_{\parallel\mathrm{N}}J_0(k_\perp\rho_s)\widehat{\mathcal{V}}_{\mathrm{N},s}\;.\end{aligned}\tag{3.85}$$

CHAPTER

Mitigation of the Cancellation Problem in Local Gyrokinetic Simulations

4

In this chapter the established mitigation technique from Chapter 3.8.5 will be implemented into the local (flux-tube) version of the Gyrokinetic Workshop (GKW). In this version GKW solves the Vlasov equation (linear or nonlinear) for the modified distribution function g [Ch. 3.8.4] As coordinates GKW uses the field aligned Hamada coordinates[8] with the coordinate set $\{s,\ \psi,\ \zeta,\ v_{\parallel},\ \mu\}$. Here, s parameterizes the length along the field lines, ψ is the radial coordinate (normalized by ρ_{th}) and ζ represents approximately the binormal coordinate. In general GKW calculates the solution of the Vlasov and field equations with a matrix vector multiplication. The solutions will be stored in the array `fdisi`, which contains the distribution g and the fields Φ_1, $A_{1\parallel}$, $B_{1\parallel}$ and other "fields" and will be updated dynamically for each timestep. For that, multiple matrices will be defined which will only act on specific elements in `fdisi`. These matricies contain terms which appear before a calculated quantity. To evolve the distribution function in time, a simple Runge Kutta scheme will be used. Additionally, in GKW there a multiple diagnostics defined, each diagnostics computes and outputs a distinct physical quantity.[18] To read more about the code GKW the reader is referred to Ref. 17 or to the manual[18].

The implementation of the mitigation technique is separated in three steps

(1) Implementation of Faraday's law into GKW,

(2) Calculation of the gyrocenter distribution function F_1 in the linear version of GKW and

(3) Calculation of the nonlinear terms with the gyrocenter distribution F_1.

The reader is referred to the branch in bibucket[12] for more in depth documentation on the process and implementation. The simulations were performed on the `emil`[20] cluster, the `festus`[21] cluster of the University Bayreuth or on one of the `btppx` machines of the TPV Chair.

4.1 Improvements

To begin, it is important to highlight the applied code improvements that were done to ensure a valid implementation of the Faraday Law into GKW.

(1) In the diagnostics part of GKW serveral subroutines and functions rely on the definition of the variable `requirements` from the module `diagnostics`. The variable `requirements` is a matrix which communicates what type of data or ghost cell needs to be provided to the diagnostic. In the previous implementation the number of columns were hard-coded into the field identifier for the gyroaveraged parallel magnetic field $\bar{B}_{1\parallel}$ with `BPAR_GA_FIELD`. This type of problem occured on multiple occasions throughout the code, most noteable in the module `dist` with `derivs_in_lin_terms` and the token array in `diagnos_generic`. Furthermore, it was found that in the code, more inconvenient structures were established. For example, the slicing of the `requirements` matrix was performend by `PHI_FIELD:BPAR_FIELD` and `PHI_GA_FIELD:BPAR_GA_FIELD`, which is again linked to hard-coded variables. To prevent any errors with future modifications, new variables and schemes are introduced in the module `global` as

- `MIN_FIELD` as the smallest number of the field identifiers,
- `MIN_GA_FIELD` as the smallest number of the gyroaverages field identifiers
- `MAX_FIELD` as the greatest number of the field identifiers,
- `MAX_GA_FIELD` as the greatest number of the gyroaverages field identifiers,
- `DISTRIBUTION` should always have the greatest number and
- `MAX_IDX_FIELD` is the greatest number, i.e. `DISTRIBUTION`.

These changes allow to implement `EPAR_FIELD` and `EPAR_GA_FIELD` as

- `EPAR_FIELD = 4`,
- `EPAR_GA_FIELD = 8`

as well as a new scheme for slicing

- `PHI_FIELD:BPAR_FIELD` replaced by `MIN_FIELD:MAX_FIELD`,
- `PHI_GA_FIELD:BPAR_GA_FIELD` replaced by `MIN_GA_FIELD:MAX_GA_FIELD`.

The field identifier for the distribution functionen F_1 changed to the number 9 and the size of the arrays or matrix is defined by `MAX_IDX_FIELD`. It is advisable to make sure that the field identifier for the distribution function is always the greatest number. Further changes were performed in the whole code to ensure the new scheme is applied. The changed code sequence in `global` is listed below

(2) Since the calculation of $E_{1\parallel}$ needs the right-hand side of the Vlasov equation $\mathcal{V}$ and the regular fields perform the calculation with the distribution function F_1, a seperation between additional and regular field equations were done. For that purpose, new the variables are introduced in `dist`, which follows the existing notation

- `nregular_fields_start` as the start of the solutions of the regular fields, i.e. Φ, $A_{1\parallel}$ and $B_{1\parallel}$, in `fdisi`,
- `nadditional_fields_start` as the start of the solutions of the additional fields, i.e. $E_{1\parallel}$, in `fdisi`,
- `nadditional_fields_end` as the end of the solutions of the regular fields in `fdisi`.

Here, `nregular_fields_start` replaces the variable `n_phi_start` to improve the code to a more general naming scheme. Note that, the declaration of the new variables have a specific place in the code and should not be changed. So, if anyone was to add a new regular field, the definition of the number of elements in `fdisi` and ghost cells should be put above the declaration of `nregular_fields_start` and `nregular_fields_end`, the same goes for additonal fields.

(3) The size of the field matrix `poisson_int` and `mat_field_diag` in the module `matdat` was implemented too big with the size of `ntot` which is the number grid points for the whole array `fdisi`. To add a more efficent way to define the size of the regular field matrices the new variable `nelem_regular_fields` is defined as `nelem_regular_fields = nf *(1 * number_of_fields)` in `dist`. Here, `nf = nsp*nx*nmu*nvpar*nmod` stands for the number of grid points for the distribution function F_1 and `number_of_fields` is an integer which is incremented for every activated field calculation. In general, `nelem_regular_fields` is always less than `ntot` which could improve the runtime of the code, since allocation of the field matrices takes less time than before. The declaration of `nelem_regular_fields` is in the same code block as `nregular_fields_start` and `nregular_fields_end` and should not be changed, since it relies heavily on the parameter `number_of_fields`.

(4) In the subroutine `calculate_fields` in `fields` the division of the diagonal parts of the regular fields was performed by a loop starting at `nregular_fields_start` and ends at the size of `mat_field_diag`. Since it was very unintuitive to start the loop not at the first element of the matrix, further investigations were done, and it was found that in `linear_terms` a unity block of the size of `nf` was added in the front of the first element of `mat_field_diag`. This code sequence was removed and with this the loop in `calculate_fields` adjusted to loop from the first element to the last element of `mat_field_diag`.

(5) The subroutine `g2f_correct` from the module `linear_terms` is renamed. Since it calculates the $A_{1\parallel}$-correction, which is the $A_{1\parallel}$-term in Equation 3.69, it was more convienent to rename the subroutine to `apar_correct`. Associated switches in the module control were renamed as well.

(6) Overall the code syntax was continuously corrected and minor mistakes were addressed as they occured.

4.2 Faraday's law in GKW

4.2.1 Implementation

Since the code is capable of parallization the inserted code is written to use the OpenMPI libary. Further subtle changes or import statements will not be stated since most are following the established stucture of $A_{1\parallel}$ and add them for $E_{1\parallel}$ into the code as well. The reader is referred to the branch in bibucket[12] for more in depth documentation on the process and implementation.

Before detailing the implementation for the calculation of $E_{1\parallel}$, the scheme of the calculation needs to be discussed. As stated in Equation (3.85) the right-hand side of the Vlasov equation $\mathcal{V}$ (RHS) is necessary for the calculation of $E_{1\parallel}$. Now, if one takes a closer look at Equations (3.69) and (3.74) it can be derived as

$$\frac{\partial g}{\partial t} = \mathcal{V} \ , \tag{4.1}$$

where g is the modified distribution. Since GKW has already implemented $\partial_t g$ as `rhs` and the Vlasov equation with the modified distribution function [Eq (3.70)] has only one additional term containing g, which is nonlinear, i.e. ignored in linear cases, `rhs` will be used as the right-hand side of the Vlasov equation in the calculation of $E_{1\parallel}$. In the next step the numerical scheme for every Runge Kutta step ($i \to i+1$) has to be considered. Figure 4.1 gives an illustration of the scheme.

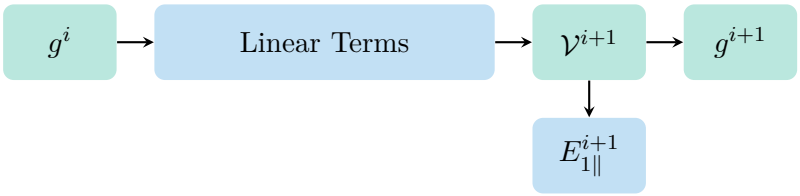

Figure 4.1: Numerical scheme used to calculate the plasma induction $E_{1\parallel}$ in GKW. First the modified distribution function g for the time step i is used to calculate the RHS $\mathcal{V}$ for the time step $i+1$, which calculates the plasma induction $E_{1\parallel}$ and distribution g for timestep $i+1$.

As shown, the order of calculations is important in the numerical scheme, i.e. first calculate the right-hand side of the Vlasov equation $\mathcal{V}$ and afterwards the induced electric field $E_{1\parallel}$.

To add the plasma induction $E_{1\parallel}$ into GKW the following changes were applied:

- The boolean input parameter `nlepar` was added in the `control` module to activate the calculation of the $E_{1\parallel}$ field. Since the simulation has to be electromagnetic, the switch for the $A_{1\parallel}$ field will also be turned on.
- In the module `dist` the identifiers for the $E_{1\parallel}$ and $\bar{E}_{1\parallel}$ are declared `iepar` and `iepar_ga`. These identifieres make it possible to access only $E_{1\parallel}$ and $\bar{E}_{1\parallel}$ in the solution `fdisi` with the use of the index function from the module `index_function`. Additionally, the grid points, ghost cells and the size of the additional field matrices are defined in the module `dist` as well.
- A new subroutine called `calculate_additional_fields` is introduced in the module fields. As stated before the calculation of the $E_{1\parallel}$ needs the RHS as argument an in the subroutine. As parameter the calculated variable `rhs` from the module `exp_integration` will be used. Additionally, the variable `rhs` has to be devided by the timestep `deltatime` from the Runge Kutta scheme, because `rhs` is the product of the right-hand side $\mathcal{V}$ and the timestep `deltatime`. Here, the timestep `deltatime` is parsed by the argument `DTIM` in `calculate_additional_fields` and originate from the module `exp_integration`. The calculation is performed in two steps:

  (1) Matrix vector multiplication of the matrix containing the integral part of $E_{1\parallel}$ with the "pure" right-hand side array `rhs/DTIM`
  `fdisi = mat_add_field_int * (rhs / DTIM)`

  (2) Division of the matrix containing the diagonal part of $E_{1\parallel}$
  `fdisi = fdisi / mat_add_field_diag`.

  To achieve the structure shown in Figure 4.1 the calculation of $E_{1\parallel}$ is performed after the subroutine `calculate_rhs` from the module `exp_integration`.
- The matricies `mat_add_field_int` and `mat_add_field_diag` are defined in the module `matdat`. Here, the matrix `mat_add_field_int` contains the linear term `faraday_int` and `mat_add_field_diag` the term `faraday_diag`. Both matrix elements are calculated in the module linear terms and are given by

$$\begin{aligned} \texttt{faraday\_int} &= -2\pi B_{\mathrm{N}} \beta_{\mathrm{ref}} \sum_s Z_s n_{\mathrm{R},s} v_{\mathrm{thR},s} \int \mathrm{d}v_{\parallel \mathrm{N}} \mathrm{d}\mu_{\mathrm{N}}\ v_{\parallel \mathrm{N}} J_0(k_\perp \rho_s) \\ \texttt{faraday\_dia} &= \left(k_{\perp \mathrm{N}}^2 + \beta_{\mathrm{ref}} \sum_s \frac{Z_s^2 n_{\mathrm{R},s}}{m_{\mathrm{R},s}} \Gamma_0(b_s) e^{-\mathcal{E}_{\mathrm{N},s}/T_{\mathrm{R},s}} \right) . \end{aligned} \tag{4.2}$$

  Note that, the 2π factor in `faraday_int` is already included in the array `intmu`[18] and will be ignored. The size of the matrices are given by `nelem_regular_fields`. During the optimization of the number of elements for `mat_add_field_int` and `mat_add_field_diag` it was found that `nelem_additional_fields` cannot be further reduced. Plausibly, the field matrices for the additional fields have to account for the number of elements for regular field matrices as well.

- To extract $E_{1\parallel}$ from `fdisi` the subroutine `get_epar` is needed in the diagnostic `diagnos_mode_struct` which outputs the data of parallel quantities. Here, `get_epar` either returns the data for the $E_{1\parallel}$ field in two columns, sorted by real and imaginary part, or two zero colums, if the `nlepar` switch is off. Additionally, the code is adjusted to the additional field and the variables `epar` and `eperp` are renamed to `ene_par` and `ene_perp`. Due to the new additional data sets and the definition of `get_epar` the testcases
  - `adiabat_collisions_momcon_ap`,
  - `chease_cf_modebox`,
  - `collisions_please_dont_break_me` and
  - `zonal_flow_sixth_order_FD`

  have to be adjusted to contain the two zero columns from $E_{1\parallel}$ in the parallel data.

4.2.2 Benchmark

To benchmark the implementation of Faraday's law with $E_{1\parallel}$ multiple linear simulations for different plasma beta β are performed. The goal is to extract the linear growth rate γ and frequency ω o the most dominant mode to compare the result for $E_{1\parallel}$ with $A_{1\parallel}$. In general a given quantity is saved in `parallel.dat` in two columns containing real and imaginary values. The rows are sorted by the species N_{sp}, binormal gird points N_{mod}, radial grid points N_x and grid points along the field line N_s and therefore $N_{\mathrm{sp}}N_{\mathrm{mod}}N_xN_s$ rows. The data stored in `parallel.dat` is defined as

$$\widehat{L}(s,t) = \exp(\gamma t + i\omega t)\widehat{L}(s) \ , \tag{4.3}$$

where $\widehat{L}(s,t)$ is the calculated quantity and $\widehat{L}(s)$ is the stored value.[18] Note that, $\widehat{L}(s,t)$ and $\widehat{L}(s)$ are complex. With Equation (4.3) one can derive the relation between $\widehat{E}_{1\parallel}$ and $\widehat{A}_{1\parallel}$ with Faraday's law [Eq. (3.76)] as

$$\begin{aligned}
\widehat{E}_{1\parallel}(s,t) &= -\partial_t \widehat{A}_{1\parallel}(s,t) \\
\exp(\gamma t + i\omega t)\widehat{E}_{1\parallel}(s) &= -\partial_t \left[\exp(\gamma t + i\omega t)\widehat{A}_{1\parallel}(s)\right] \\
\widehat{E}_{1\parallel}(s) &= -(\gamma + i\omega)\widehat{A}_{1\parallel}(s) \\
\widehat{E}^{\mathrm{R}}_{1\parallel}(s) + i\widehat{E}^{\mathrm{I}}_{1\parallel}(s) &= -(\gamma + i\omega)\left(\widehat{A}^{\mathrm{R}}_{1\parallel}(s) + i\widehat{A}^{\mathrm{I}}_{1\parallel}(s)\right)
\end{aligned} \tag{4.4}$$

$$\Rightarrow \boxed{\begin{aligned}
\widehat{E}^{\mathrm{R}}_{1\parallel}(s) &= -\gamma\widehat{A}^{\mathrm{R}}_{1\parallel}(s) + \omega\widehat{A}^{\mathrm{I}}_{1\parallel}(s) \\
\widehat{E}^{\mathrm{I}}_{1\parallel}(s) &= -\omega\widehat{A}^{\mathrm{R}}_{1\parallel}(s) - \gamma\widehat{A}^{\mathrm{I}}_{1\parallel}(s)
\end{aligned}}$$

For the plasma beta following values are investigated

$$\beta \in [0.0,\ 0.2,\ 0.4,\ 0.6,\ 0.8,\ 1.0,\ 1.1,\ 1.2,\ 1.4,\ 1.6]\,\% \ . \tag{4.5}$$

The values will be set with the parameter `beta` in the input file. As base input file the cyclone benchmark case (CBC) with s-α geometry provided by the GKW Team was used. Here, s-α geometry implies that the flux surfaces is being circular and has a small inverse aspect ratio r/R_0, where r is the radius of the flux surface and R_0 the major radius [Ch. 2.2]. The input file can be found in the GKW repository under `doc/input/cyclone`. Here, the input parameters were adjusted for linear β scan and are displayed in Table 4.1.

Additionally following parameter were set

- `NON_LINEAR` = `.false.` to enable linear simulations,
- `nlepar` = `.true.` to enable the calculatation of $E_{1\parallel}$,
- `io_format` = `'hdf5` output data to `hdf5` format,
- `gama_tol` = $1 \cdot 10^{-5}$ defines tolerance for linear growth rate γ,
- `adiabatic_electrons` = `.false.` to enable kinetic electrons,
- `mode_box` = `.false.` deactivates 2D mode grid and
- $k_\zeta \rho = 0.3$ defines "poloidal" wave vector which corresponds roughly to the position of the maximum of the nonlinear transport spectrum in GKW.

`DTIM`	`NTIME`	`NAVERAGE`	N_{mod}	N_x	N_s	$N_{v_\parallel}$	N_μ	N_{sp}	`nperiod`
0.01	2000	100	1	1	288	64	16	2	5

Table 4.1: Adjusted input parameter for linear β scan: Initial time step size `DTIM`, number of iterations of `NAVERAGE` `NTIME`, number of timesteps between re-normalisation `NAVERAGE`, number of binormal grid points N_{mod}, number of radial gird points N_x,number of grid points along the magnetic field N_s, number of parallel velocity grid points $N_{v_\parallel}$, numbe magnetic moment grid points N_μ, number of species N_{sp} and `nperiod` as integer which specify the length of the field line.

The result of the linear β scan can be seen in Figure 4.2. The obtained data shows agreement with Ref. 4 and 11, although GENE normalises with speed of sound and GKW normalise by the thermal velocity v_{th}, the values are $\sqrt{2}$ times smaller. Furthermore, by comparing the beta scan in Ref. 4 or 11 and Figure 4.2 the transition from ion temperature gradient mode (ITG) to kinetic ballooning mode (KBM) are located at notably different values of plasma beta β. This behaviour is due to different values for the wave vector $k_\zeta \rho$ and the resolution of parallel velocity grid $N_{v_\parallel}$. The comparison between the plasma induction $E_{1\parallel}$ and vector potential $A_{1\parallel}$ yields the implementation of the $E_{1\parallel}$ field equation as successful. An overall camparison is shown in Figure 4.3 and for a more detailed look for different plasma beta values the reader is referred to Appendix 6.1.1.

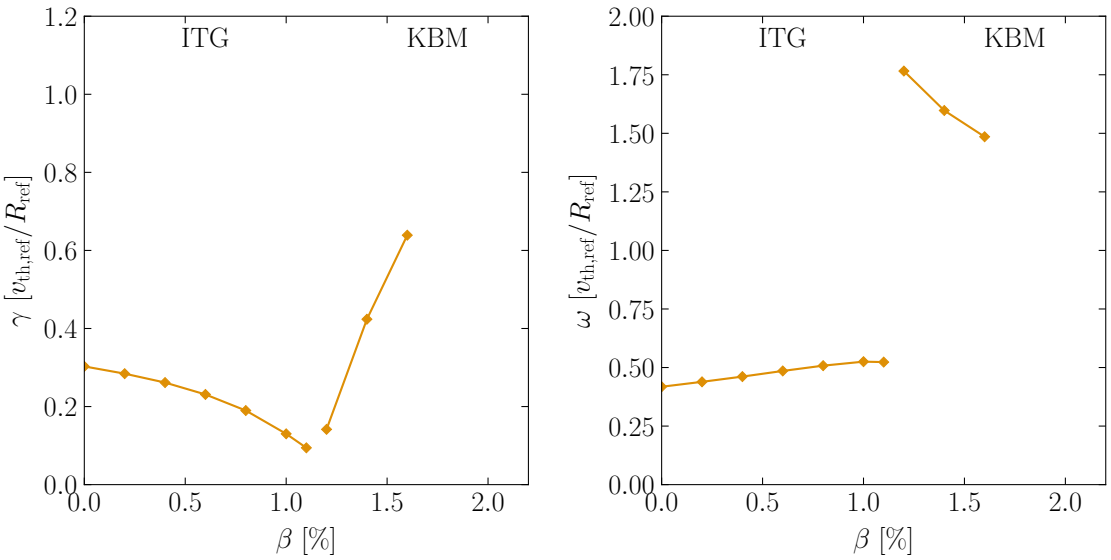

Figure 4.2: Growth rate γ and frequency ω for different plasma beta β. Here, (ITG) stands for ion temperature gradient modes and (KBM) for kinetic ballooning modes.

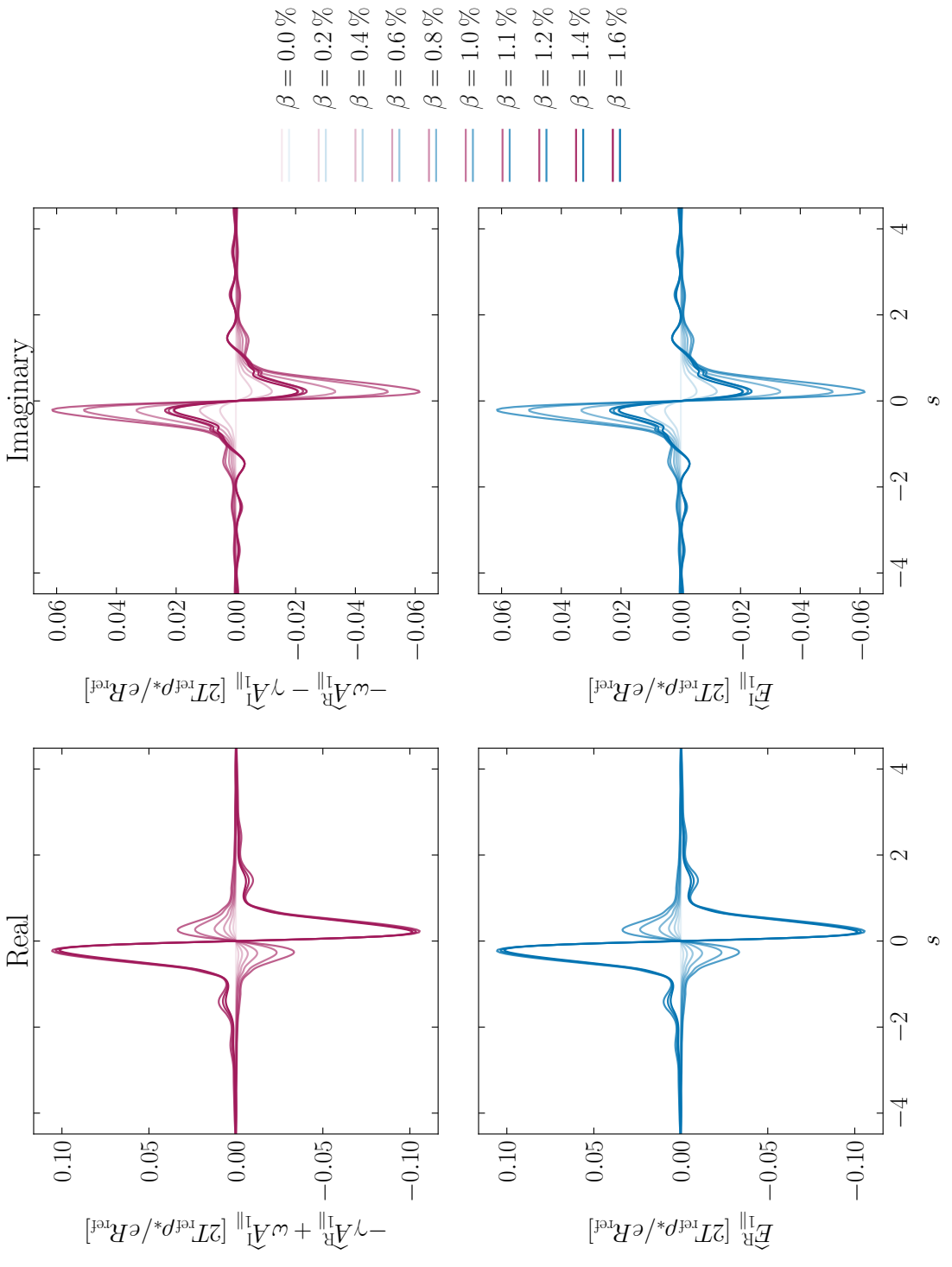

Figure 4.3: Comparision between real and imaginary part of the plasma induction $E_{1\parallel}$ and vector potential $A_{1\parallel}$ for different plasma beta values for the g-verison of GKW.

4.3 Linear f-Version of GKW

4.3.1 Implementation

As stated in Chapter 3.8.4 the current version of GKW implements the Vlasov equation with the use of the modified distribution function g. To preserve the established structure of the code and to calculate the distribution function F_1 the right-hand side $\mathcal{V}$ is transformed. This version will be from now on called the *f-version* and the old version the *g-version*. To recall the right-hand side of the Vlasov equation $\mathcal{V}$ is definded as

$$\frac{\partial g}{\partial t} = \mathcal{V} \tag{4.6}$$

which is implemented numerically with Runge Kutta (one timestep $(i \to i+1)$) as

$$g^{i+1} = g^i + \Delta t \cdot \left(\mathcal{V}^{i+1}\right) \ . \tag{4.7}$$

To transform the established scheme to the distribution function F_1, Equation 3.78 has to be considered and is given by

$$\frac{\partial F_1}{\partial t} = \mathcal{V} + \frac{Zev_\parallel}{T} J_0 E_{1\parallel} F_\mathrm{M} \ , \tag{4.8}$$

where $J_0 E_{1\parallel} = \bar{E}_{1\parallel}$ in the local simulation and the term will be called $E_{1\parallel}$*-correction*, which can be written normalised and Fourier transformed as

$$\frac{\partial \widehat{F}_{1\mathrm{N},s}}{\partial t_\mathrm{N}} = \widehat{\mathcal{V}}_\mathrm{N} + \frac{2Zv_\mathrm{thR} v_{\parallel\mathrm{N}}}{T_\mathrm{R}} J_0 \widehat{E}_{1\parallel\mathrm{N}} F_\mathrm{MN} \ . \tag{4.9}$$

Here, the numerical Runge Kutta scheme can be expressed as

$$F_1^{i+1} = F_1^i + \Delta t \cdot \left(\mathcal{V}^{i+1} + \frac{Zev_\parallel}{T} J_0 E_{1\parallel}^{i+1}\right) \ . \tag{4.10}$$

Note that, to transform the gyrocenter distribution function F_1, applying the $E_{1\parallel}$-correction to the RHS is enough. The overall new numerical scheme can be seen in Figure 4.4.

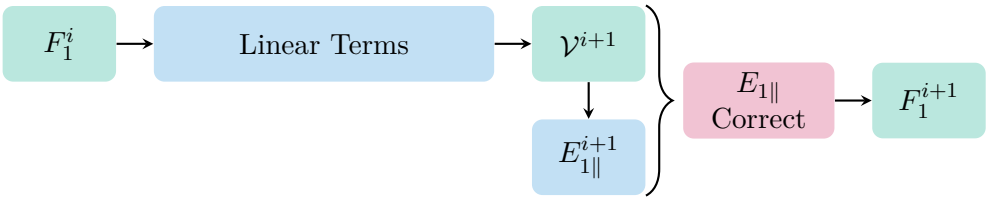

Figure 4.4: Numerical scheme used to calculate the distribution function F_1 in the linear f-version of GKW. The gyrocenter distribution function F_1 for the time step i is used to calculate the RHS $\mathcal{V}$ for the time step $i+1$, which calculates the plasma induction $E_{1\|}$ for timestep $i+1$. The plasma induction will be used to apply the $E_{1\|}$-correction to the RHS $\mathcal{V}$, which calculates the distribution F_1 for time step $i+1$

To implement the f-version the following changes will be applied to GKW:

- An boolean input parameter called `f_version` is defined in module `control`, which switches `nlepar` and `nlapar` on for the calculation of F_1. The solution `fdisi` stores the gyrocenter distribution F_1 instead of the modified distribution g. In the subroutine `control_initt` adding additonal switches for the f-version of GKW.
- The matrix `matrhs4f` (RHS for F_1) is introduced in the module `matdat` with `nelem_rhs4f` number of elements defined in the module `dist` is possible.
- The elements itself are set in the subroutine `epar_correct` which originates from the subroutine `apar_correct`. The difference is the swap of sign for the matrix elements and the use of $E_{1\|}$ identifiers instead of $A_{1\|}$.
- The RHS then is corrected after the calculation of the $E_{1\|}$ field in the subroutine `calculate_rhs` in the module `exp_integration`. Here, the loop method was used as the calculation of the new RHS needs 50% longer with the `usmv` subroutine. Note that the $E_{1\|}$-correction has to be multiplied with the time step `deltatime` to have the correct expression for the Runge Kutta scheme.
- The function `get_f_from_g`, which returns F_1 by applying the $A_{1\|}$-correction to the distribution g, is modified to return `fdisi` without the $A_{1\|}$-correction. Additionally, any code using the $A_{1\|}$-correction will be deactivated for the f-version and the definition of the matrix `matg2f` is supressed as well to save disk space during simulation.
- The field equation of the perturbated vector potential $A_{1\|}$ has to be adjusted, since it is the only field equation with significantly changes introduced by the substitution of the modified distribution g [Ch. 3.8.4 & Ch. 3.8.3]. For that an "if statement" for the f-version is introduced into the subroutine `ampere_dia` in the module `linear_terms` which deactivates the skin term. Additionally, a second exception was added to set the `ampere_dia` to zero if a zero mode ($k_\perp = 0$) is initialized. This prevents large matrix elements caused by the division by zero, since `ampere_dia` equals $k_\perp^2$ in the f-version. As already mentioned in Chapter 3.8 the other field equations are still valid for the f-version.

4.3.2 Benchmark

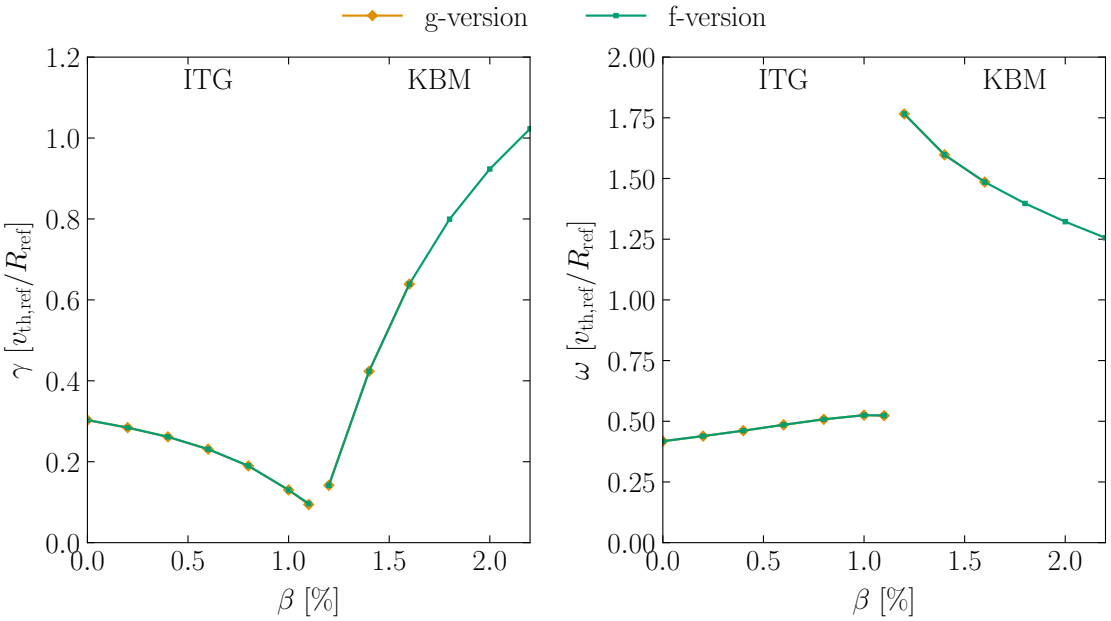

Figure 4.5: Growth rate γ and frequency ω for different plasma beta β. Here, (ITG) stands for ion temperature gradient modes, (TEM) for trapping electron modes and (KBM) for kinetic ballooning modes.

Again the same benchmark as in Chapter 4.2.2 will be performed with the same simulation setup. The plasma beta was varied between

$$\beta \in [0.0,\ 0.2,\ 0.4,\ 0.6,\ 0.8,\ 1.0,\ 1.1,\ 1.2,\ 1.4,\ 1.6,\ 1.8,\ 2.0,\ 2.2]\,\% \ . \tag{4.11}$$

To verify that the f-version of GKW calculates the field equation for the vector potential $A_{1\parallel}$ correctly, since the field equation was changed (compare Eq. (3.68) and (3.73)), the vector potential is compared a second time with the plasma induction $E_{1\parallel}$ [Fig. 4.6]. Here, the comparison shows that the field equations are implemented successfully. For a more detailed look for different plasma beta values the reader is referred to Appendix 6.1.2. A performance measurement was also executed to investigate the run time of the f-version compared to the g-version in local linear simulations. Here, the run time for each explicit timestep is compared for different plasma beta values on a btppx maschine of the TPV chair with 12 processors selected. This comparison yields, that the f-version adds approximately 10 % of run time for each timestep. Additionally, the resolutions (N_s, $N_{v_\parallel}$ and N_μ) for different plasma beta is halfed and comparing the g-version and the f-version results in no difference, meaning that the resolution changes, i.e. the discretization of the grid points, do not make the simulatons less exact.

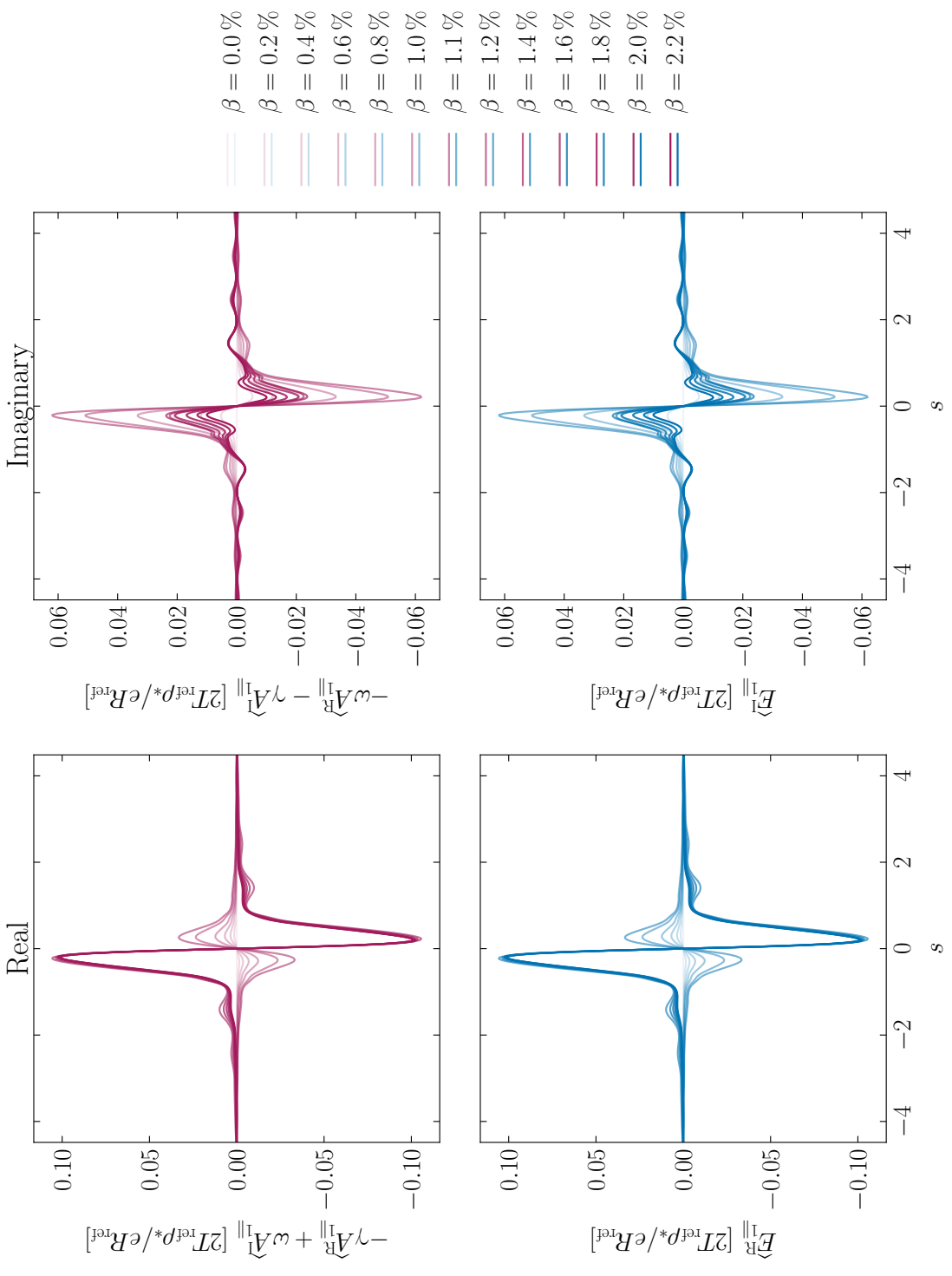

Figure 4.6: Comparision between real and imaginary part of the plasma induction $E_{1\parallel}$ and vector potential $A_{1\parallel}$ for different plasma beta values for the f-verison of GKW.

4.3.3 Mitigation of the Cancellation Problem in linear Simulations

One of the main goals of this thesis is to mitigate the cancellation problem [Ch. 3.8.4] in local simulations. The error of problem scales with $\sim \beta/k_\perp^2$ [15]. Therefore, it was investigated if the new f-version improves the code run time for long perpendicular turbulent length scales $k_\perp$. First, a $k_\perp$ scan was performed with the g-version of GKW and CBC parameters for $\beta = 0.8\,\%$ to find the transition between stable simulations and unstable ones. Here, it was found that the simulation is unstable for $k_\perp = 0.027\,1/\rho_{\mathrm{th,ref}}$. Unfortunately, the f-version is also unstable for the exact same value of $k_\perp$. Additionally, to the CBC parameters simulations the ASDEX-Upgrade input parameters (AUG) were performed with the same result. The g-version as well as the f-version both are unstable for the same $k_\perp$. Considering the $A_{1\parallel}$ equation in the g-version and the $E_{1\parallel}$ equation f-version

$$\begin{aligned}
&\left(k_{\perp\mathrm{N}}^2 + \beta_{\mathrm{ref}} \sum_s \frac{Z_s^2 n_{\mathrm{R},s}}{m_{\mathrm{R},s}} \Gamma_0(b_s) e^{-\mathcal{E}_{\mathrm{N},s}/T_{\mathrm{R},s}}\right) \widehat{A}_{1\parallel\mathrm{N}} = \\
&2\pi B_{\mathrm{N}} \beta_{\mathrm{ref}} \sum_s Z_s n_{\mathrm{R},s} v_{\mathrm{thR},s} \int \mathrm{d}v_{\parallel\mathrm{N}} \mathrm{d}\mu_{\mathrm{N}}\; v_{\parallel\mathrm{N}} J_0(k_\perp \rho_s) \widehat{g}_{\mathrm{N},s} \\
&\left(k_{\perp\mathrm{N}}^2 + \beta_{\mathrm{ref}} \sum_s \frac{Z_s^2 n_{\mathrm{R},s}}{m_{\mathrm{R},s}} \Gamma_0(b_s) e^{-\mathcal{E}_{\mathrm{N},s}/T_{\mathrm{R},s}}\right) \widehat{E}_{1\parallel\mathrm{N}} = \\
&-2\pi B_{\mathrm{N}} \beta_{\mathrm{ref}} \sum_s Z_s n_{\mathrm{R},s} v_{\mathrm{thR},s} \int \mathrm{d}v_{\parallel\mathrm{N}} \mathrm{d}\mu_{\mathrm{N}}\; v_{\parallel\mathrm{N}} J_0(k_\perp \rho_s) \widehat{\mathcal{V}}_{\mathrm{N},s}
\end{aligned} \tag{4.12}$$

it shows both equations have the same structure. In the modified distribution function g is a "hidden" $A_{1\parallel}$-term and in $\mathcal{V}$ is a "hidden" $E_{1\parallel}$-term additionaly the skin term is calculated in both equations numerically and with the same scheme as the integrals. Possibly, improvement of the mitigation technique relies on the size of the plasma induction $E_{1\parallel}$. For that the $E_{1\parallel}$ field has to be significantly smaller than the $A_{1\parallel}$ field. However, a direct comparison yields no significant difference. To conclude the cancellation problem still occurs in linear local simulations and the introduced mitigation technique does not work.

4.4 Nonlinear f-Version of GKW

4.4.1 Implementation

Until now only the linear terms of the gyrokinetic equations were discussed. To complete the transformation to the f-version of GKW the nonlinear terms have to be considered as well. Because of the substitution of the modified distribution function g the nonlinear terms

$$\mathbf{v}_\chi \cdot \nabla F_1 \qquad - \frac{F_\mathrm{M}}{T} \mathbf{v}_{\bar{B}_{1\perp}} \cdot (Ze\nabla\bar{\Phi} + \mu\nabla\bar{B}_{1\parallel})$$

were replaced with $\mathbf{v}_\chi \cdot \nabla g$. To implement the nonlinear terms again, the definition of the modified distribution into the already implemented nonlinear terms subroutine is inserted. This results in the following relation

$$\begin{aligned}
\mathbf{v}_\chi \cdot \nabla g &= \mathbf{v}_\chi \cdot \nabla \left(F_1 + \frac{Zev_\parallel}{T} \bar{A}_{1\parallel} F_\mathrm{M} \right) \\
&= \mathbf{v}_\chi \cdot \nabla F_1 + \frac{ZeF_\mathrm{M}}{T} \mathbf{v}_\chi \cdot \nabla (v_\parallel \bar{A}_{1\parallel}) \\
&= \mathbf{v}_\chi \cdot \nabla F_1 + \frac{ZeF_\mathrm{M}}{T} \mathbf{v}_{\bar{B}_{1\perp}} \cdot \left(\nabla\bar{\Phi} - \nabla(v_\parallel \bar{A}_{1\parallel}) + \frac{\mu}{Ze} \nabla \bar{B}_{1\parallel} \right) \\
&= \mathbf{v}_\chi \cdot \nabla F_1 + \frac{F_\mathrm{M}}{T} \mathbf{v}_{\bar{B}_{1\perp}} \cdot (Ze\nabla\bar{\Phi} + \mu\nabla\bar{B}_{1\parallel}) \ ,
\end{aligned} \tag{4.13}$$

although the term with $\mathbf{v}_\chi \cdot \nabla F_\mathrm{M}$ is neglected due to order of $\rho_\star^2$. The numerical scheme used in the nonlinear f-version of GKW can be seen in Figure 4.7.

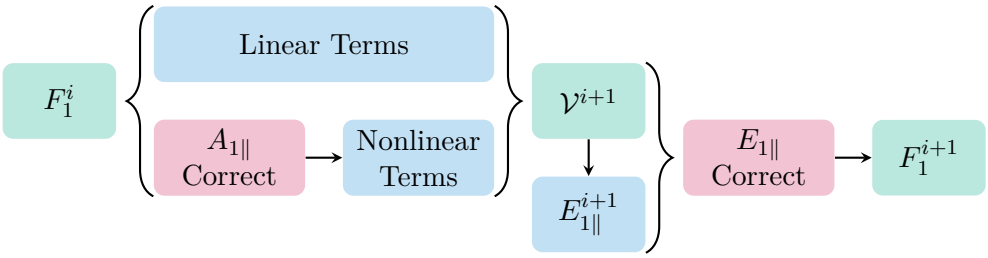

Figure 4.7: Numerical scheme used to calculate the distribution function F_1 in the nonlinear f-version of GKW. The gyrocenter distribution function F_1 for the time step i is used to calculate the RHS $\mathcal{V}$ for the time step $i+1$. Here, the $A_{1\parallel}$-correction is applied to the distribution F_1 to calculate the nonlinear terms, which contribute the RHS $\mathcal{V}$ as well.

To calculate the nonlinear terms with GKW the following changes to the code are applied:

- Since the introduction of the f-version of GKW, the solution array `fdisi` stores F_1, so the $A_{1\parallel}$-term has to be added to distribution stored in `fdisi`, i.e. apply the $A_{1\parallel}$-correction. The $A_{1\parallel}$-correction to receive F_1 from g is already implemented into GKW with the matrix `matg2f` with its elements defined in the subroutine `apar_correct`. To apply the $A_{1\parallel}$-correction to F_1 the signs of the matrix element of `matg2f` have to be swaped. To distinguish, between the f-version and the g-version the matrix elements are written into the matrix `matf2g` instead of using `matg2f`.
- The $A_{1\parallel}$-correction is performed via loop over the elements of `fdisi` in the subroutine `add_non_linear_terms` and saved in the temporary distribution array `fdis_tmp`. The array `fdis_tmp` will be used to calculate the nonlinear terms. It is important to ensure the usage of `fdis_tmp` since in the f-version the distribution F_1 gets used for further calculation and should not be changed.

The changes are valid if the input parameter `f_version` and `non_linear` are active and local simulations are performed.

4.4.2 Benchmark

To benechmark the nonlinear f-version of GKW the geometry of the CBC parameters are changed to circular geometry and the box size of the simulation is increased in binormal direction. Here, circular geometry implies that the flux surfaces are circular and concentric with the poloidal flux being a function of the radial coordinate Ψ.[18] The change to the box size increases the wave vector $k_\perp$, which is directly linked to the cancellation problem. To increase the box size the following relation will be used to change the input parameter accordingly

$$\begin{aligned} N_x(L_\psi) &= ((N_x(1)-1)\cdot L_\psi)+1 \\ N_{\mathrm{mod}}(L_\zeta) &= ((N_{\mathrm{mod}}(1)-1)\cdot L_\psi)+1 \\ \texttt{ikxspace}(L_\psi, L_\zeta) &= \texttt{ikxspace}(1,1)\cdot L_\psi/L_\zeta \ , \end{aligned} \tag{4.14}$$

where L_ψ relates to the box size in radial direction, L_ζ to the boxsize in binormal direction and `ikxspace` determines the spacing between the different modes. The box size will be given bei the notation $L_\psi \times L_\zeta$. For nonlinear simulations the following box sizes will be investigated

$$L_\psi \times L_\zeta \in [1\times 1, 1\times 2, 1\times 3, 1\times 6] \ .$$

Unfortunately, due to high demand on the `emil` cluster or `festus` cluster and some unresolved problems within GKW, it was not possible to finish the nonlinear investigation in time. Available data suggests that by comparing the fluxes between the nonlinear g-version and f-version, the implementation is valid, but this is only a trend.

CHAPTER

5

Conclusion

In this thesis the cancellation problem is investigated and a technique to mitigate it was implemented in the local (flux-tube) version of GKW. This mitigation technique introduces an additional electomagnetic field through Faraday's law, the plasma induction $E_{1\parallel}$. During the implementation process, GKW was transformed from the so called g-version to the new f-version, which directly calculates the unmodified distribution function. This f-version will be used for future investigation of the cancellation problem in the global version of GKW.

During the benchmark of the f-version of GKW it was found that the cancellation problem could not be mitigated with the same technique in local linear simulations. The nonlinear benchmark shows a trend that the implementation is valid but no further asssumptions could be made with the data available in this thesis. Further investigations into the nonlinear f-version might yield a solution to the cancellation problem in local simulations.

CHAPTER

6

Appendix

6.1 Comparision between $E_{1\parallel}$ and $A_{1\parallel}$ for various plasma beta

6.1.1 For the g-version of GKW

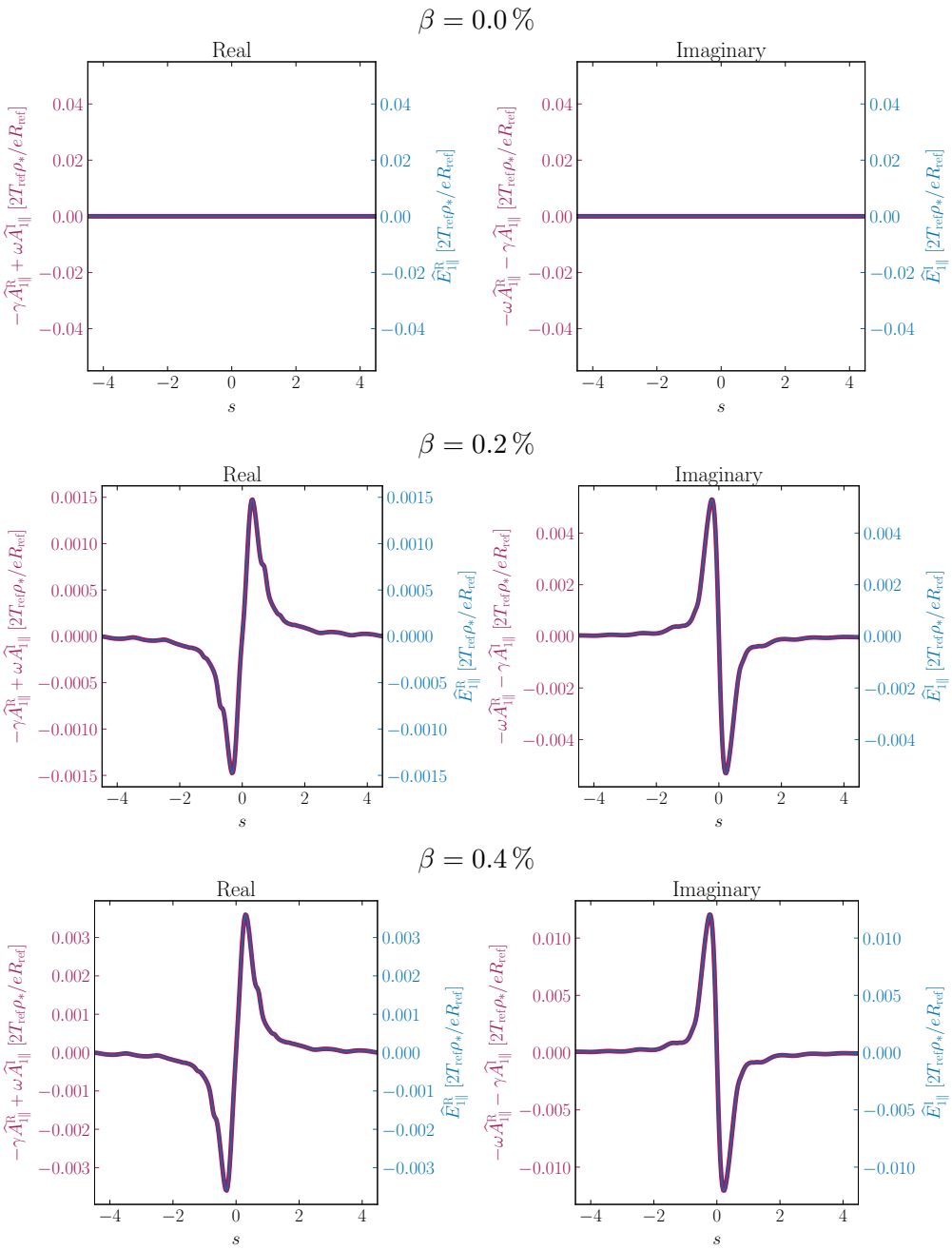

$\beta = 0.6\,\%$

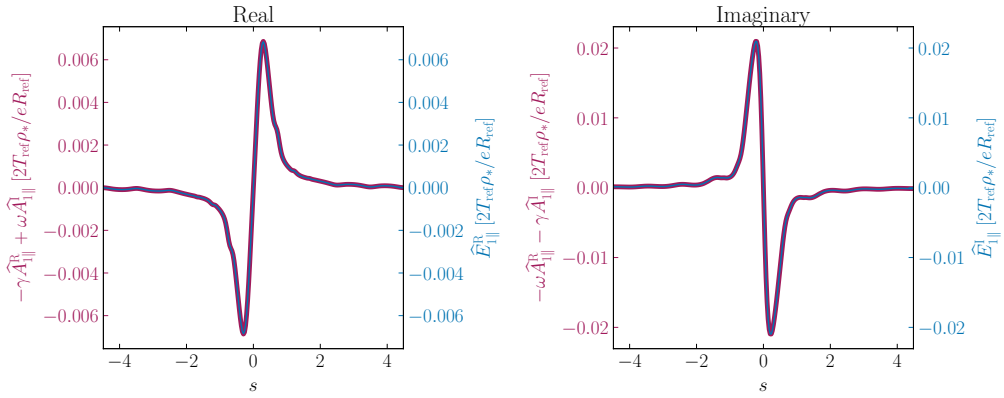

$\beta = 0.8\,\%$

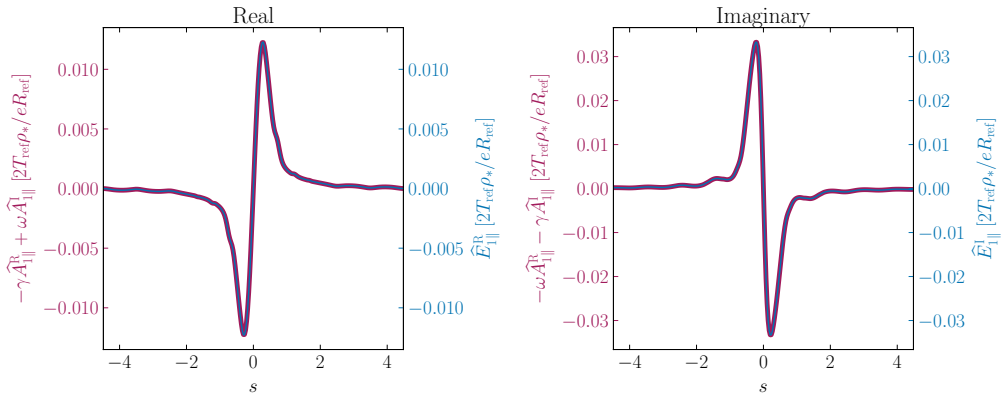

$\beta = 1.0\,\%$

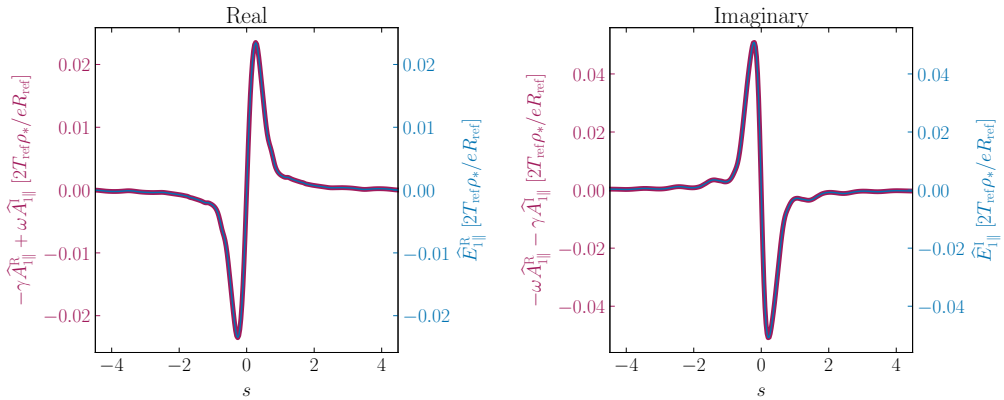

$\beta = 1.1\,\%$

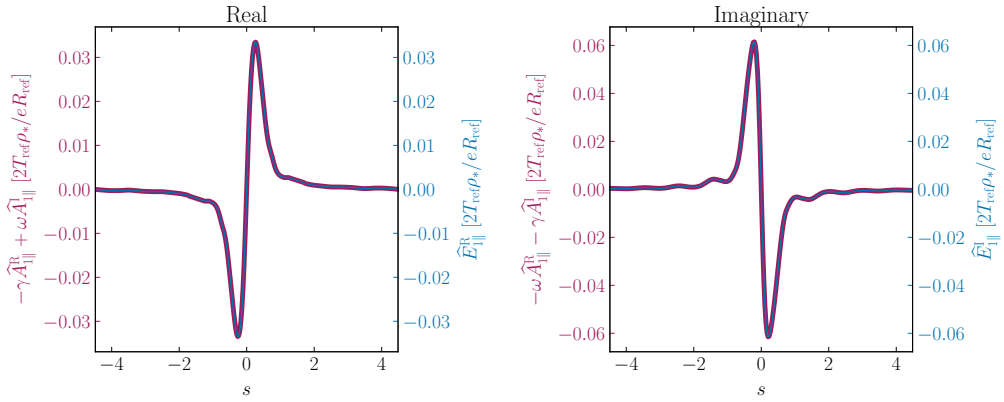

$\beta = 1.2\,\%$

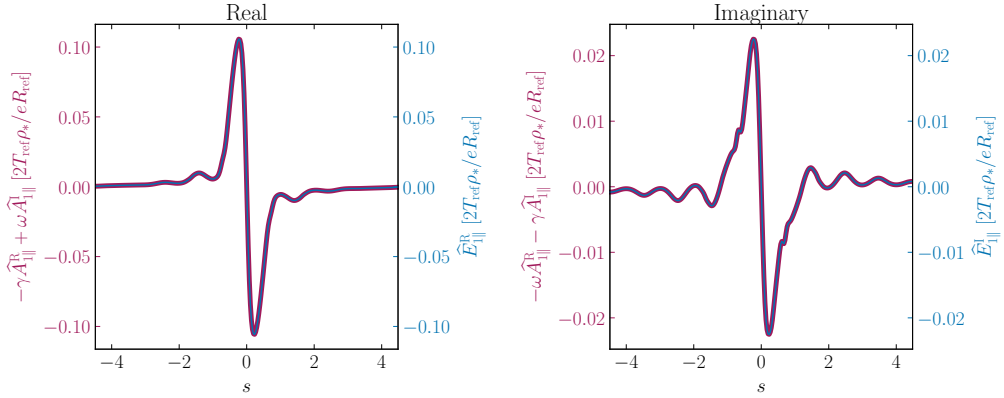

$\beta = 1.4\,\%$

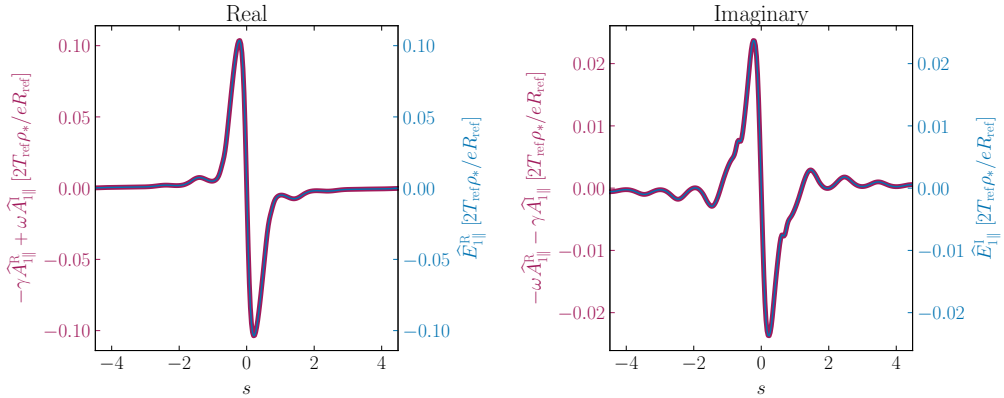

$\beta = 1.6\,\%$

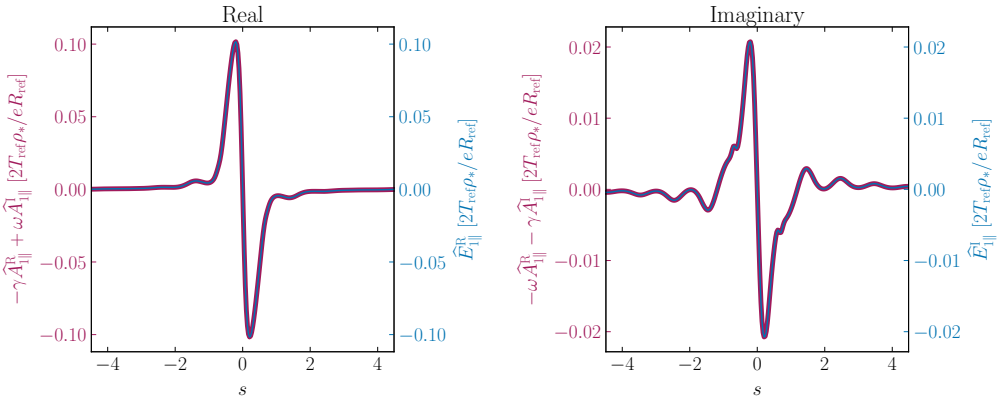
Real
Imaginary
$-\gamma\widehat{A}_{1\parallel}^{\mathrm{R}} + \omega\widehat{A}_{1\parallel}^{\mathrm{I}}\ [2T_{\mathrm{ref}}\rho_s/eR_{\mathrm{ref}}]$
$\widehat{E}_{1\parallel}^{\mathrm{R}}\ [2T_{\mathrm{ref}}\rho_s/eR_{\mathrm{ref}}]$
$-\omega\widehat{A}_{1\parallel}^{\mathrm{R}} - \gamma\widehat{A}_{1\parallel}^{\mathrm{I}}\ [2T_{\mathrm{ref}}\rho_s/eR_{\mathrm{ref}}]$
$\widehat{E}_{1\parallel}^{\mathrm{I}}\ [2T_{\mathrm{ref}}\rho_s/eR_{\mathrm{ref}}]$
0.10
0.05
0.00
−0.05
−0.10
0.02
0.01
0.00
−0.01
−0.02
−4
−2
0
2
4
s

6.1.2 For the f-version of GKW

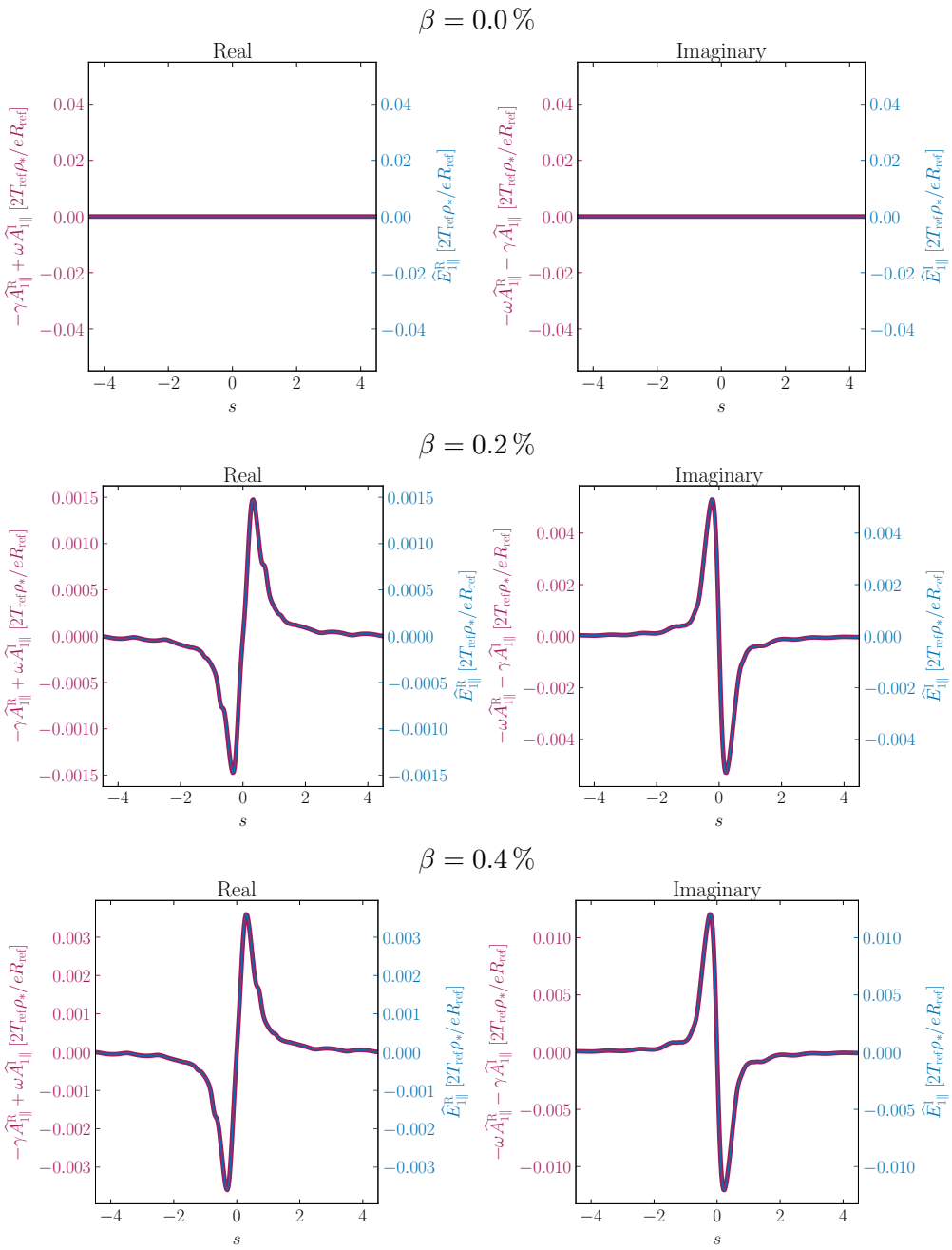

$\beta = 0.6\,\%$

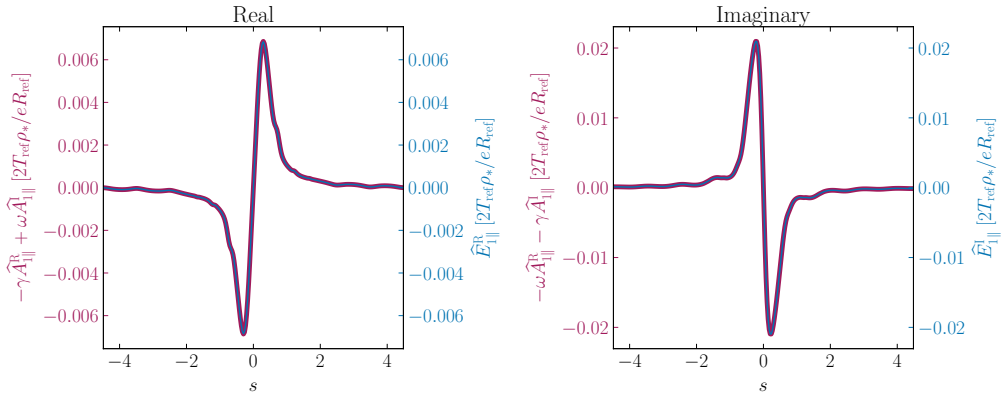

$\beta = 0.8\,\%$

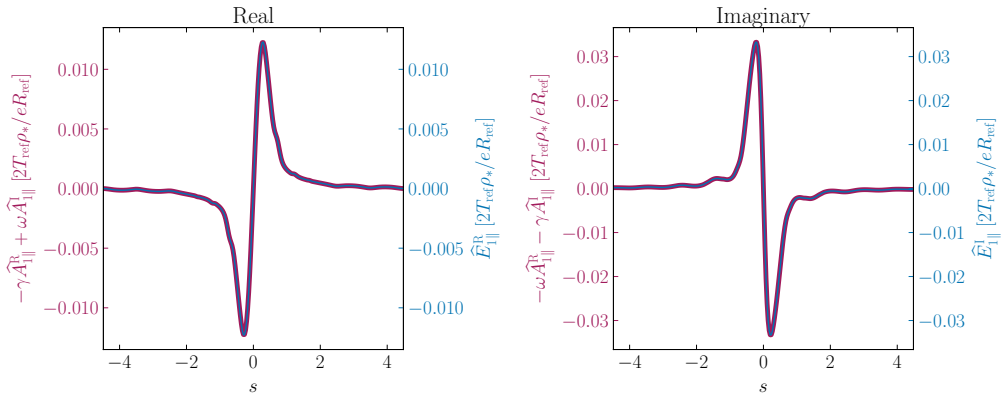

$\beta = 1.0\,\%$

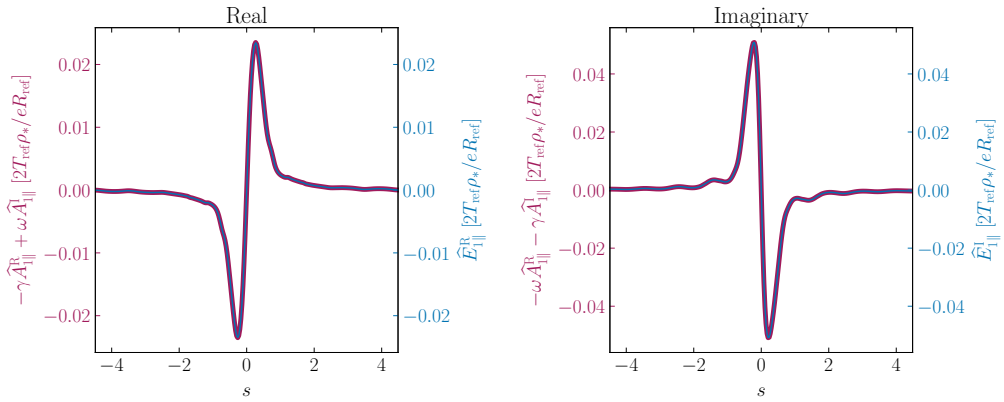

$\beta = 1.1\,\%$

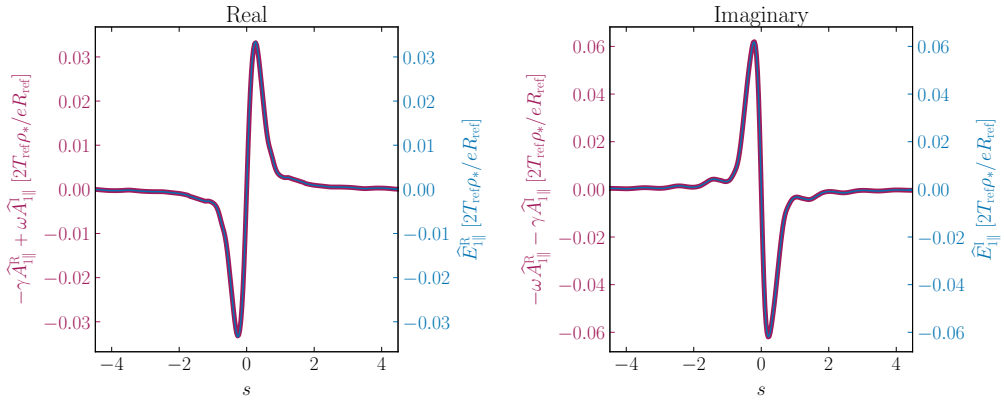

$\beta = 1.2\,\%$

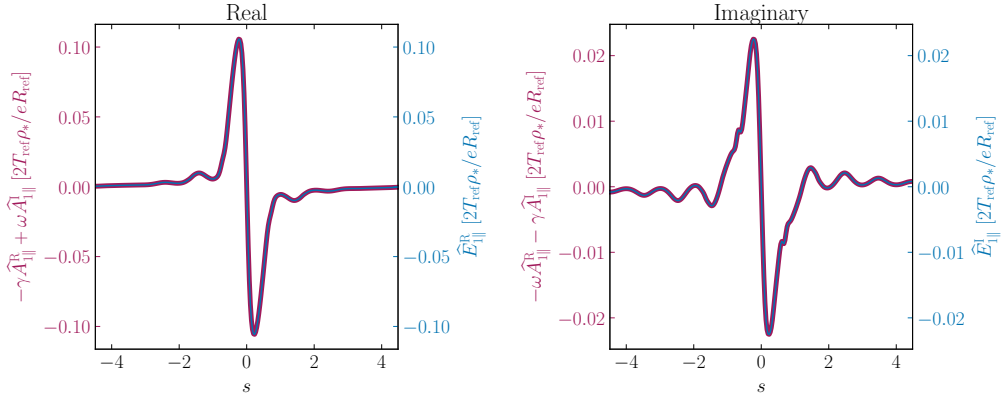

$\beta = 1.4\,\%$

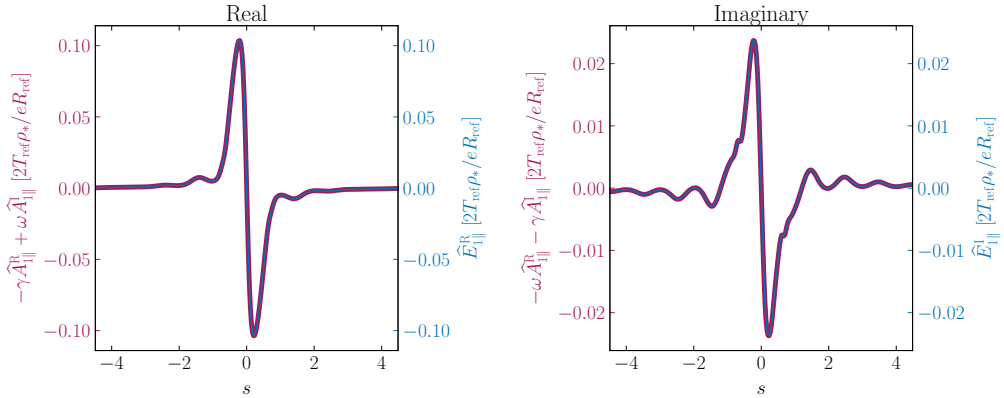

$\beta = 1.6\,\%$

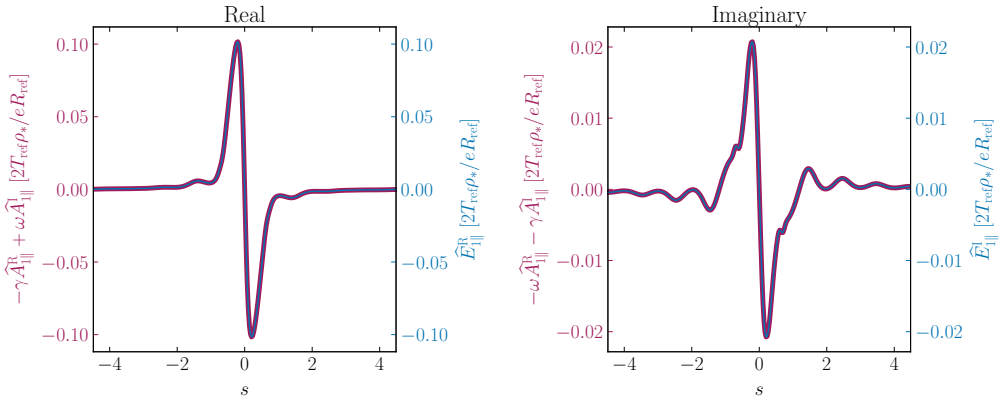

$\beta = 1.8\,\%$

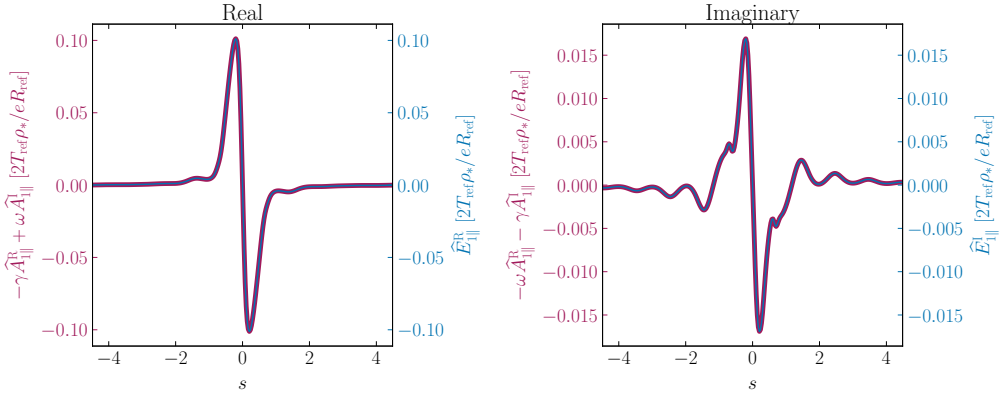

$\beta = 2.0\,\%$

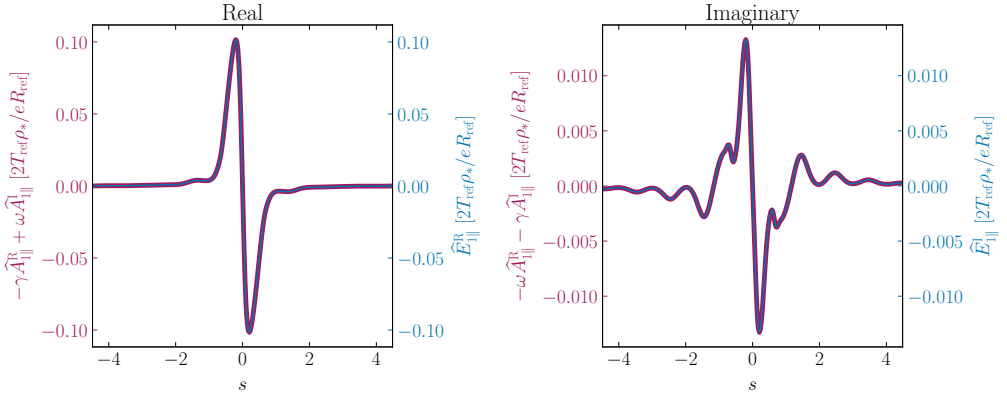

$\beta = 2.2\,\%$

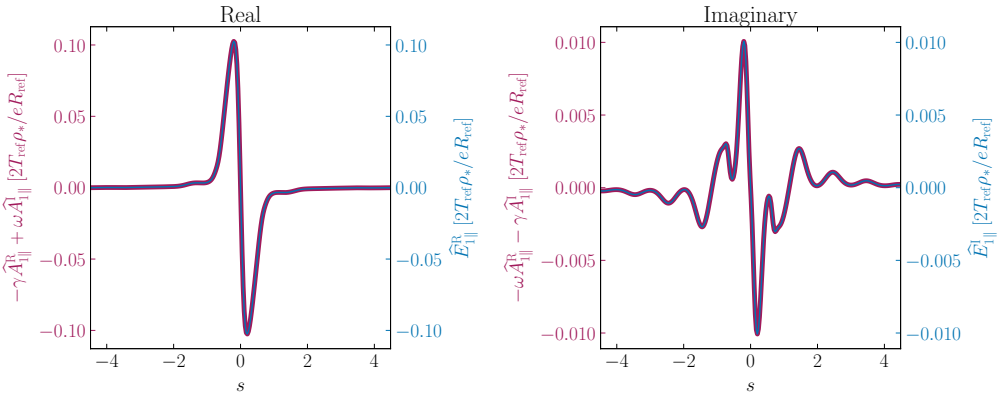
Real
Imaginary
$-\gamma\widehat{A}_{1\parallel}^{\mathrm{R}} + \omega\widehat{A}_{1\parallel}^{\mathrm{I}}\ [2T_{\mathrm{ref}}\rho_*/eR_{\mathrm{ref}}]$
$\widehat{E}_{1\parallel}^{\mathrm{R}}\ [2T_{\mathrm{ref}}\rho_*/eR_{\mathrm{ref}}]$
$-\omega\widehat{A}_{1\parallel}^{\mathrm{R}} - \gamma\widehat{A}_{1\parallel}^{\mathrm{I}}\ [2T_{\mathrm{ref}}\rho_*/eR_{\mathrm{ref}}]$
$\widehat{E}_{1\parallel}^{\mathrm{I}}\ [2T_{\mathrm{ref}}\rho_*/eR_{\mathrm{ref}}]$
0.10
0.05
0.00
−0.05
−0.10
0.010
0.005
0.000
−0.005
−0.010
−4
−2
0
2
4
s

CHAPTER

7

Bibliography

[1] Barton, Justin E., Wehner, William P., Schuster, Eugenio, Felici, Federico & Sauter, Olivier 2015 Simultaneous closed-loop control of the current profile and the electron temperature profile in the TCV tokamak. In *2015 American Control Conference (ACC)*, pp. 3316–3321. Chicago, IL, USA: IEEE.

[2] Brizard, A. J. & Hahm, T. S. 2007 Foundations of nonlinear gyrokinetic theory. *Reviews of Modern Physics* **79** (2), 421–468.

[3] Chen, Yang & Parker, Scott 2001 Gyrokinetic turbulence simulations with kinetic electrons. *Physics of Plasmas* **8** (5), 2095–2100.

[4] Crandall, Paul Charles 2019 *Collisional and Electromagnetic Physics in Gyrokinetic Models*. PhD thesis.

[5] Cummings, J. C. 1995 *Gyrokinetic Simulation of Finite-Beta and Self-Generated Sheared-Flow Effects on Pressure-Gradient-Driven Instabilities*. PhD thesis, Princeton University.

[6] Dannert, Tilman 2004 *Gyrokinetische Simulation von Plasmaturbulenz mit gefangenen Teilchen und elektromagnetischen Effekten*. PhD thesis.

[7] Garbet, X., Idomura, Y., Villard, L. & Watanabe, T.H. 2010 Gyrokinetic simulations of turbulent transport. *Nuclear Fusion* **50** (4), 043002.

[8] Hamada, Shigeo 1962 Hydromagnetic equilibria and their proper coordinates. *Nuclear Fusion* **2** (1-2), 23–37.

[9] Kaufmann, Michael 2013 *Plasmaphysik und Fusionsforschung*. Wiesbaden: Springer Fachmedien Wiesbaden.

[10] Krommes, John A. & Kim, Chang-Bae 2000 Interactions of disparate scales in drift-wave turbulence. *Physical Review E* **62** (6), 8508–8539.

[11] Leppin, Leonhard Andrew 2024 *Turbulence Simulations of the High Confinement Mode Pedestal in Tokamak Fusion Experiments*. PhD thesis, Technische Universität München.

[12] Lippert, M. 2024 GKW Branch feature/feature_Epar_extension. https://bitbucket.org/gkw/gkw/branch/feature/feature_Epar_extension.

[13] Maurer, Maurice 2020 *GENE-3D - a Global Gyrokinetic Turbulence Code for Stellarators and Perturbed Tokamaks*. PhD thesis.

[14] Merlo, Gabriele 2016 *Flux-Tube and Global Grid-Based Gyrokinetic Simulations of Plasma Microturbulence and Comparisons with Experimental TCV Measurements*. PhD thesis.

[15] Mishchenko, Alexey, Bottino, Alberto, Hatzky, Roman, Sonnendrücker, Eric, Kleiber, Ralf & Könies, Axel 2017 Mitigation of the cancellation problem in the gyrokinetic particle-in-cell simulations of global electromagnetic modes. *Physics of Plasmas* **24** (8), 081206.

[16] Naitou, Hiroshi, Tsuda, Kenji, Lee, W W & Sydora, R D 1995 Gyrokinetic simulation of internal kink modes .

[17] Peeters, A.G., Camenen, Y., Casson, F.J., Hornsby, W.A., Snodin, A.P., Strintzi, D. & Szepesi, G. 2009 The nonlinear gyro-kinetic flux tube code GKW. *Computer Physics Communications* **180** (12), 2650–2672.

[18] Peeters, A. G., Buchholz, R., Camenen, Y., Casson, F. J., Grosshauser, S. R., Hornsby, W. A., Manas, P., Migliano, P., Siccinio, M., Snodin, A. P., Strintzi, D., Sung, T., Szepesi, G. & Zarzoso, D. 2016 GKW how and why.

[19] Peeters, A. G., Strintzi, D., Camenen, Y., Angioni, C., Casson, F. J., Hornsby, W. A. & Snodin, A. P. 2009 Influence of the centrifugal force and parallel dynamics on the toroidal momentum transport due to small scale turbulence in a tokamak. *Physics of Plasmas* **16** (4), 042310.

[20] Schelter, Ingo 2024 Emil (btrzx1). https://www.bzhpc.uni-bayreuth.de/de/keylab/Cluster/btrzx1_page/index.html.

[21] Schelter, Ingo 2024 Festus. https://www.bzhpc.uni-bayreuth.de/de/keylab/Cluster/btrzx24_page/index.html.

[22] Stroth, Ulrich 2018 *Plasmaphysik: Phänomene, Grundlagen und Anwendungen*. Berlin, Heidelberg: Springer Berlin Heidelberg.

[23] Szepesi, G. 2023 Derivation of the fully electro-magnetic, non-linear, gyrokinetic Vlasov–Maxwell equations in a rotating frame of reference for GKW with Lie transform perturbation method .

[24] Told, D. 2012 *Fluctuations of the Electron Temperature Due to Plasma Turbulence in an Internal Transport Barrier Discharge of the TCV Tokamak.*. PhD thesis, University Ulm.

[25] Wesson, J. 2004 *Tokamaks*, 3. Oxford University Press.

Eidesstattliche Erklärung

Hiermit erkläre ich, Manuel Lippert, dass ich die vorliegende Arbeit selbständig und ohne Benutzung anderer als der angegebenen Hilfsmittel angefertigt habe. Alle Stellen,

die wörtlich oder sinngemäß aus veröffentlichten oder nicht veröffentlichten Schriften entnommen wurden, sind als solche kenntlich gemacht. Die Arbeit hat in gleicher oder

ähnlicher Form noch keiner anderen Prüfungsbehörde vorgelegen.

Bayreuth, den 30.06.2023

_____

Manuel Lippert